Atmos. Chem. Phys., 12, 3527–3557, 2012
www.atmos-chem-phys.net/12/3527/2012/
doi:10.5194/acp-12-3527-2012

Atmospheric Chemistry and Physics

Observed and simulated time evolution of HCl, $ClONO_2$, and HF total column abundances

R. Kohlhepp[1], R. Ruhnke[1], M. P. Chipperfield[2], M. De Mazière[3], J. Notholt[4], S. Barthlott[1], R. L. Batchelor[5,6], R. D. Blatherwick[7], Th. Blumenstock[1], M. T. Coffey[6], P. Demoulin[8], H. Fast[9], W. Feng[2], A. Goldman[6], D. W. T. Griffith[10], K. Hamann[1], J. W. Hannigan[6], F. Hase[1], N. B. Jones[10], A. Kagawa[11,12], I. Kaiser[1], Y. Kasai[11], O. Kirner[13], W. Kouker[1], R. Lindenmaier[5], E. Mahieu[8], R. L. Mittermeier[9], B. Monge-Sanz[2], I. Morino[14], I. Murata[15], H. Nakajima[16], M. Palm[4], C. Paton-Walsh[10], U. Raffalski[17], Th. Reddmann[1], M. Rettinger[18], C. P. Rinsland[19,†], E. Rozanov[20,21], M. Schneider[1], C. Senten[3], C. Servais[8], B.-M. Sinnhuber[4,1], D. Smale[22], K. Strong[5], R. Sussmann[18], J. R. Taylor[5,23], G. Vanhaelewyn[3], T. Warneke[4], C. Whaley[5], M. Wiehle[1], and S. W. Wood[22]

[1]Karlsruhe Institute of Technology (KIT), Institute for Meteorology and Climate Research (IMK-ASF), Karlsruhe, Germany
[2]Institute for Climate and Atmospheric Science, School of Earth and Environment, University of Leeds, Leeds, UK
[3]Belgian Institute for Space Aeronomy (BIRA-IASB), Brussels, Belgium
[4]Institute of Environmental Physics, University of Bremen, Bremen, Germany
[5]Department of Physics, University of Toronto, Toronto, Ontario, Canada
[6]National Center for Atmospheric Research (NCAR), Boulder, CO, USA
[7]Department of Physics and Astronomy, University of Denver, Denver, CO, USA
[8]Institute of Astrophysics and Geophysics, University of Liège, Liège, Belgium
[9]Environment Canada, Toronto, Ontario, Canada
[10]Centre for Atmospheric Chemistry, University of Wollongong, Wollongong, Australia
[11]National Institute of Information and Communications Technology, Tokyo, Japan
[12]Fujitsu FIP Corporation, Tokyo, Japan
[13]Karlsruhe Institute of Technology (KIT), Steinbuch Centre for Computing, Karlsruhe, Germany
[14]Center for Global Environmental Research, National Institute for Environmental Studies (NIES), Japan
[15]Department of Environmental Studies, Graduate School of Environmental Studies, Tohoku University, Japan
[16]Atmospheric Environment Division, National Institute for Environmental Studies (NIES), Japan
[17]Swedish Institute of Space Physics (IRF), Kiruna, Sweden
[18]Karlsruhe Institute of Technology (KIT), Institute for Meteorology and Climate Research (IMK-IFU), Garmisch-Partenkirchen, Germany
[19]NASA Langley Research Center, Hampton, VA, USA
[20]ETH Zürich, Institute for Atmospheric and Climate Science (IACETH), Zürich, Switzerland
[21]Physical-Meteorological Observatory, World Radiation Center, Davos, Switzerland
[22]National Institute of Water and Atmospheric Research Ltd (NIWA), Lauder, New Zealand
[23]National Ecological Observatory Network (NEON), Boulder, CO, USA
[†]deceased

Correspondence to: R. Kohlhepp (regina.kohlhepp@kit.edu)

Received: 28 September 2011 – Published in Atmos. Chem. Phys. Discuss.: 7 December 2011
Revised: 15 March 2012 – Accepted: 2 April 2012 – Published: 12 April 2012

Abstract. Time series of total column abundances of hydrogen chloride (HCl), chlorine nitrate ($ClONO_2$), and hydrogen fluoride (HF) were determined from ground-based Fourier transform infrared (FTIR) spectra recorded at 17 sites belonging to the Network for the Detection of Atmospheric Composition Change (NDACC) and located between 80.05° N and 77.82° S. By providing such a near-global overview on ground-based measurements of the two major

stratospheric chlorine reservoir species, HCl and $ClONO_2$, the present study is able to confirm the decrease of the atmospheric inorganic chlorine abundance during the last few years. This decrease is expected following the 1987 Montreal Protocol and its amendments and adjustments, where restrictions and a subsequent phase-out of the prominent anthropogenic chlorine source gases (solvents, chlorofluorocarbons) were agreed upon to enable a stabilisation and recovery of the stratospheric ozone layer. The atmospheric fluorine content is expected to be influenced by the Montreal Protocol, too, because most of the banned anthropogenic gases also represent important fluorine sources. But many of the substitutes to the banned gases also contain fluorine so that the HF total column abundance is expected to have continued to increase during the last few years.

The measurements are compared with calculations from five different models: the two-dimensional Bremen model, the two chemistry-transport models KASIMA and SLIMCAT, and the two chemistry-climate models EMAC and SOCOL. Thereby, the ability of the models to reproduce the absolute total column amounts, the seasonal cycles, and the temporal evolution found in the FTIR measurements is investigated and inter-compared. This is especially interesting because the models have different architectures. The overall agreement between the measurements and models for the total column abundances and the seasonal cycles is good.

Linear trends of HCl, $ClONO_2$, and HF are calculated from both measurement and model time series data, with a focus on the time range 2000–2009. This period is chosen because from most of the measurement sites taking part in this study, data are available during these years. The precision of the trends is estimated with the bootstrap resampling method. The sensitivity of the trend results with respect to the fitting function, the time of year chosen and time series length is investigated, as well as a bias due to the irregular sampling of the measurements.

The measurements and model results investigated here agree qualitatively on a decrease of the chlorine species by around $1\,\%\,yr^{-1}$. The models simulate an increase of HF of around $1\,\%\,yr^{-1}$. This also agrees well with most of the measurements, but some of the FTIR series in the Northern Hemisphere show a stabilisation or even a decrease in the last few years. In general, for all three gases, the measured trends vary more strongly with latitude and hemisphere than the modelled trends. Relative to the FTIR measurements, the models tend to underestimate the decreasing chlorine trends and to overestimate the fluorine increase in the Northern Hemisphere.

At most sites, the models simulate a stronger decrease of $ClONO_2$ than of HCl. In the FTIR measurements, this difference between the trends of HCl and $ClONO_2$ depends strongly on latitude, especially in the Northern Hemisphere.

1 Introduction

Short-lived reactive inorganic chlorine (e.g. Cl and ClO) is released in the stratosphere via photo-dissociation of chlorinated source gases by UV radiation (e.g. chlorofluorocarbons (CFCs), hydrochlorofluorocarbons (HCFCs), carbon tetrachloride (CCl_4), methyl chloride (CH_3Cl), methyl chloroform (CH_3CCl_3), and halons). Reactive chlorine plays a crucial role in the thinning of the stratospheric ozone layer and particularly in polar ozone depletion as it is involved in ozone-destroying catalytic cycles (Molina and Rowland, 1974; Crutzen et al., 1978). In the 1970s and 1980s, the emission of anthropogenic halogenated source gases characterised by a strong ozone depletion potential (ODP) increased massively. So in order to stabilise the stratospheric ozone layer and enable its recovery, the Montreal Protocol and its amendments and adjustments have been progressively implemented to reduce or even stop the production and release of the important chlorinated source gases.

Figure 1 shows the time development of the mean global surface volume mixing ratios of total organic chlorine (CCl_y) and total organic fluorine (CF_y) according to the halocarbon scenarios that were used as boundary conditions for the model simulations, between 1992 and 2010. Additionally, their relative annual growth rates are shown. CCl_y is defined here as 3 CFC-11 + 2 CFC-12 + 3 CFC-113 + 2 CFC-114 + CFC-115 + 4 CCl_4 + 3 CH_3CCl_3 + HCFC-22 + 2 HCFC-141b + HCFC-142b + Halon-1211 + CH_3Cl and CF_y is represented by CFC-11 + 2 CFC-12 + 3 CFC-113 + 4 CFC-114 + 5 CFC-115 + 2 HCFC-22 + HCFC-141b + 2 HCFC-142b + 2 Halon-1211 + 3 Halon-1301 + 2 Halon-1202 + 4 Halon-2402. According to the A1 scenario from WMO (2007), CCl_y is assumed to have reached its tropospheric maximum in 1993, whereas CF_y is expected to have reached a plateau with a small positive growth rate of about 0.1 % per year in 2010 (Fig. 1). The older scenario Ab from WMO (2003) assumes CCl_y to have reached its maximum only in 1995. In contrast, CF_y peaks earlier than in the A1 scenario, already in 2005, so that the growth rate in the Ab scenario in 2010 is already negative. A small part of the difference between the two scenarios probably results from the fact that in the WMO (2003) Ab scenario, Halon-2402 and Halon-1202 are not considered.

Once released from chlorinated source gases (CCl_y), chlorine atoms undergo a number of reactions in the stratosphere forming different species which are summarised as the total inorganic chlorine budget (Cl_y = HCl + $ClONO_2$ + ClO + 2 Cl_2O_2 + OClO + 2 Cl_2 + Cl + HOCl + BrCl). The largest contribution to Cl_y comes from the reservoir species HCl and $ClONO_2$. However, it is the shorter-lived, highly reactive ClO_x species (i.e. Cl + ClO + 2 Cl_2O_2) that efficiently destroy ozone.

In addition to chlorine atoms, fluorine is released by the decomposition of CFCs and HCFCs. However, in contrast to chlorine, fluorine forms long-lived substances such as COF_2

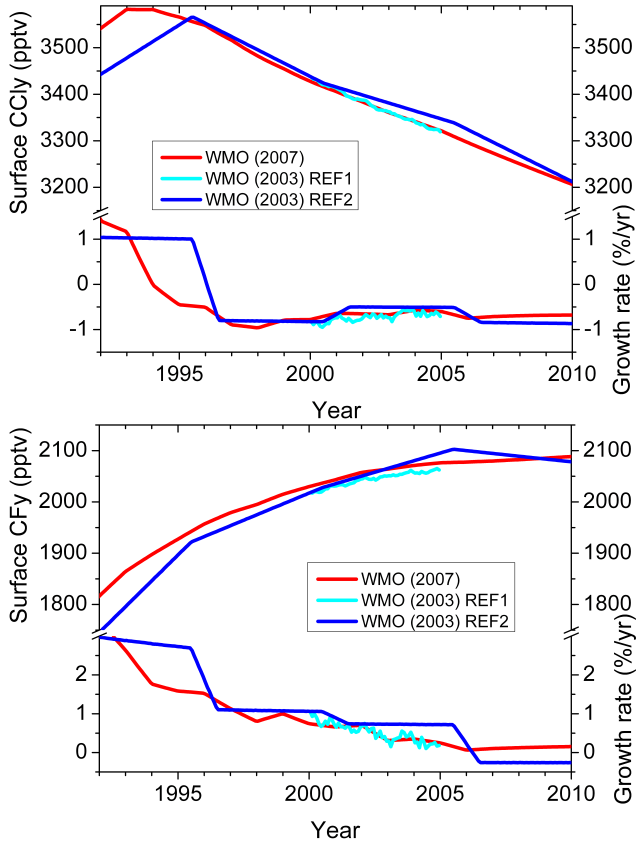

Fig. 1. Time series of monthly mean CCl_y (top) and CF_y (bottom) surface volume mixing ratios (in pptv) and growth rates (in % per year) from different halocarbon scenarios between 1992 and 2010. The one called "WMO (2003) REF2" corresponds to the scenario Ab in WMO (2003) and was used by KASIMA and the 2-D model. The "WMO (2003) REF1" time series of CCl_y and CF_y are based on that same scenario until the year 2000, but were corrected by additional measurements between 2000 and 2004. It was used by SOCOL. The "WMO (2007)" scenario is the one called A1 in WMO (2007) and was used by SLIMCAT and EMAC in this study.

and ultimately HF whose only known sink is transport to the troposphere followed by rainout. Due to its long stratospheric lifetime, fluorine, and in particular HF, is not involved in catalytic ozone destruction. It is often used as a tracer for stratospheric dynamics and transport, and hence as a reference for chemically more active trace gases like HCl (Chipperfield et al., 1997). Because fluorine is also contained in CFC substitutes, the HF total column abundance is expected to have continued increasing during the time range considered in the present study.

Thus, measurements of the time development of the reservoir species (HCl and $ClONO_2$ for the inorganic chlorine and HF for the inorganic fluorine) provide a means of verifying the effectiveness of the above-mentioned international regulations.

There have been several investigations of HCl trends from long-term ground-based measurements (Zander et al., 1987; Rinsland et al., 1991; Wallace and Livingston, 1991; Wallace et al., 1997). As they were performed before the Montreal Protocol and its amendments took effect, they report increasing HCl total column abundances. Later studies confirmed stratospheric HCl or total Cl_y to have reached a plateau at the end of the 1990s and to be decreasing since (e.g., Newchurch et al., 2003; Froidevaux et al., 2006; Lary et al., 2007).

In the investigation by Rinsland et al. (2003), time series of HCl and $ClONO_2$ from Fourier transform infrared (FTIR) total column measurements at 9 stations belonging to the Network for the Detection of Atmospheric Composition Change (NDACC) until 2001 were compared with HALOE data at 55 km and calculations from a 2-D model. The measurements agreed on a stabilisation of the stratospheric inorganic chlorine content so that Rinsland et al. (2003) were able to confirm the effectiveness of the Montreal Protocol and amendments. The FTIR measurements within NDACC have been continued until present, and more stations have joined the network. Therefore, the present study is able to continue and extend the investigations of Rinsland et al. (2003) by reporting measurements at 17 sites until the end of 2009. The primary question addressed is whether the expected decrease of the total global inorganic chlorine abundance can be confirmed now with the FTIR measurements. Furthermore, five atmospheric chemistry models were included in the study in order to investigate and inter-compare their ability to reproduce the HCl, $ClONO_2$, and HF total column amounts, their seasonal cycles and their temporal evolution, as measured by the FTIR instruments.

In the framework of the SPARC CCMVal (2010) initiative, a comparison between different chemistry-climate models (CCMs) was performed for HCl and $ClONO_2$. The two CCMs taking part in the present study, EMAC and SOCOL, were also involved in this activity. The CCM calculations were compared with FTIR measurements above the Jungfraujoch and with satellite data sets with respect to the mean annual cycle, mean profiles and total column abundances. So the present study extends the SPARC CCMVal (2010) comparison with respect to additional geolocations and compares the CCM results of EMAC and SOCOL with those of other kinds of models (a 2-D model and two chemistry-transport models, CTMs).

This paper does not aim at explaining in detail differences between models or between models and measurements. Such an analysis requires much more detailed investigations, which are beyond the scope of this study. Instead, it intends to show the global inorganic chlorine decrease seen in the FTIR measurements at 17 NDACC sites, the increase in HF, and to analyse the overall ability of different state-of-the-art atmospheric chemistry models to reproduce these measurements.

An overview of the measurements and models is given in Sect. 2 and 3, respectively. Section 4 compares the time

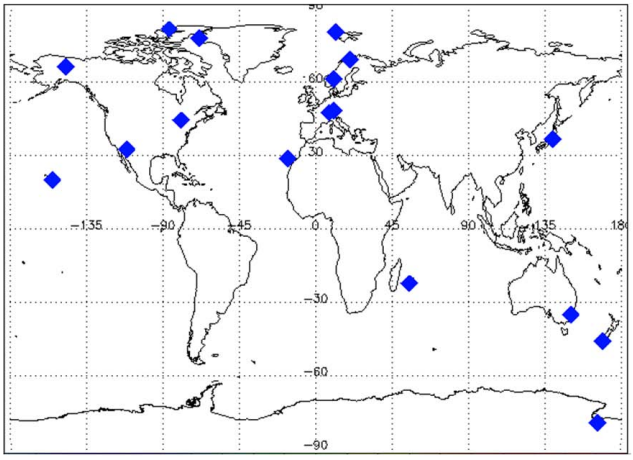

Fig. 2. Geographical distribution of the measurement sites.

series of measurements and models with respect to the mean differences between the data sets and also the mean seasonal cycle and its amplitude of the three gases. The trends of HCl, $ClONO_2$, and HF are presented in Sect. 6, but before, an investigation of the dependency of the trend results on some influencing factors is made (Sect. 5). The results are discussed in Sect. 7 and concluding remarks are given in Sect. 8.

2 Instrumentation

The observational data used in this paper were obtained from ground-based solar absorption measurements of high-spectral-resolution Fourier transform infrared (FTIR) spectrometers operated at 17 sites. They all belong to the Network for the Detection of Atmospheric Composition Change (NDACC; http://www.ndacc.org) and are located between 77.82° S and 80.05° N (see Table 1 and Fig. 2). For these measurements, the atmosphere must be free of clouds and the sun needs to be above the horizon. This implies that during polar night, no measurements are possible. Of course, this dependency on direct sunlight leads to an irregular sampling of the measurements, with considerable gaps especially during the winter at the polar sites.

The spectrometers cover the spectral range approximately 600 to 4300 cm^{-1}. In the network, it is common practice to record spectra within limited spectral bands, using a set of appropriate optical bandpass filters, in order to improve the signal-to-noise ratio. The spectral range is covered with two liquid-nitrogen-cooled detectors, namely an Indium-Antimonide (InSb) detector for the short wavelength part of the range and a Mercury-Cadmium-Telluride (MCT) detector for the long wavelength end of the range.

The high-resolution spectra include many distinct and overlapping absorption lines of a large number of atmospheric constituents. The area under the absorption lines provides information about the total abundance of the absorber gas along the line-of-sight. The spectral line shape gives additional information about the vertical distribution of the absorber in the atmosphere, based on the pressure-broadening characteristics of the line. The vertical distribution can be retrieved with limited resolution only. The so-called inversion of the spectra, to derive the vertical distribution or total column abundance of the target absorber gas from the spectra, generally uses one or a few selected spectral micro-windows. The purpose is to optimise the information content regarding the target gas and to minimise the impact of interfering species. The retrievals are based on a non-linear least squares line-by-line fit of the spectra. The more recent retrieval algorithms use a semi-empirical implementation of the optimal estimation method developed by Rodgers (2000). Only a few different retrieval codes are used within the NDACC infrared community, namely SFIT1 and SFIT2, PROFFIT and GFIT. SFIT1 and SFIT2 were developed jointly at the NASA Langley Research Center, Hampton, VA, United States, the National Center for Atmospheric Research (NCAR) at Boulder, CO, United States, and the National Institute of Water and Atmospheric Research (NIWA) at Lauder, New Zealand (Rinsland et al., 1998). SFIT1 is the older version, which does not retrieve any vertical profile information: it only performs a scaling of the a priori vertical profile. PROFFIT was developed at the Institute for Meteorology and Climate Research of the Karlsruhe Institute of Technology (KIT), and it was demonstrated that the results are equivalent to those derived with SFIT2 (Hase et al., 2004; Duchatelet et al., 2010). GFIT was developed by G. Toon at the Jet Propulsion Laboratory and performs a profile scaling similar to SFIT1 (Washenfelder et al., 2006).

The data analysis needs corresponding pressure/temperature profiles: These are taken from the National Center for Environmental Prediction (NCEP) (Lait et al., 2005) or from local or nearby radiosonde data (see supplement to the present publication). The spectroscopic parameters of the absorption lines are usually taken from the HITRAN database (Rothman et al., 1992, 1998, 2003, 2005), or from the ATMOS line list (Brown et al., 1996).

Since the retrieval of vertical profile information is based on the absorption line shapes, it is fundamental to know the instrumental line shape function (ILS) precisely. Therefore, absorption spectra of HBr in a cell at low pressure are regularly recorded. These spectra can also be used as a proxy for comparison since the HBr cells have identical origins (Coffey et al., 1998). The analysis of the resulting HBr absorption line shape, usually done with the program LINEFIT (Hase et al., 1999), yields precise knowledge of the instrument's alignment and the associated instrumental line shape function.

Different kinds of FTIR instruments have been used for the measurements analysed in this study (please see the description of the sites below), called Bruker 120M, 120HR, and 125HR, and Bomem DA8. The instrumental differences between the Bruker spectrometers are small, especially

Table 1. Overview of the geographical coordinates of the 17 sites and the time ranges covered by the HCl, $ClONO_2$, and HF measurements.

Measurement site	Latitude	Longitude	Altitude a.s.l. (m)	HCl meas. since	$ClONO_2$ meas. since	HF meas. since	Meas. used until
Eureka, Canada	80.05° N	86.42° W	610	1997	1997	1997	2009
Ny Ålesund, Svalbard, Norway	78.92° N	11.93° E	15	1992	1992	1992	2009
Thule, Greenland, Denmark	76.53° N	68.74° W	225	1999	1999	1999	2009
Kiruna, Sweden	67.84° N	20.41° E	419	1996	1996	1996	2009
Poker Flat, Alaska, USA	65.12° N	147.43° W	610	1999		1999	2004
Harestua, Norway	60.20° N	10.8° E	596	1994	1994	1994	2009
Zugspitze, Germany	47.42° N	10.98° E	2964	1995	1996	1995	2009
Jungfraujoch, Switzerland	46.55° N	7.98° E	3580	1984	1986	1984	2009
Toronto, Canada	43.66° N	79.4° W	174	2002		2002	2009
Tsukuba, Japan	36.05° N	140.12° E	31	1998		1998	2009
Kitt Peak, Arizona, USA	31.90° N	111.6° W	2090	1981	1980	1980	2009
Izaña, Tenerife, Spain	28.30° N	16.48° W	2367	1999	1999	1999	2009
Mauna Loa, Hawaii, USA	19.54° N	155.58° W	3397	1991		1995	2009
Réunion Island, France	21.80° S	55.5° E	50	2004		2004	2009
Wollongong, Australia	34.45° S	150.88° E	30	1996	1996	1996	2009
Lauder, New Zealand	45.04° S	169.68° E	370	1990	1990	1992	2009
Arrival Heights, Antarctica	77.82° S	166.65° E	250	1992	1997	1997	2009

between 120HR and 125HR. The latter is the newer version with improved electronics which in the end helps to reduce the noise in the spectra. The 120M instrument is the mobile version which is therefore smaller and more compact than the 120HR. In general, it is more difficult to adjust the 120M than the 120HR spectrometer, which may lead to a slightly worse ILS of the 120M. However, this would affect mostly the profile retrievals, not the total column abundances dealt with in this study. So there are no significant discrepancies expected between the different Bruker instruments. Furthermore, when a new instrument was installed at one site, if possible, an intercomparison was performed with the old one so that the here presented data sets can be assumed to show self-consistent time series. The discrepancies between a Bruker 125HR and a Bomem DA8 instrument were investigated in detail for the total column abundances of the three gases analysed here by e.g. Batchelor et al. (2010) and were found to amount to less than 3.5 %.

Concerning the vertical averaging kernels, the corresponding height-dependent sensitivity of the retrieval, the degrees of freedom for signal, and the overall errors associated with the measurements, no detailed information is given here. It can be found in the references given for every site, or other publications, for example in Kohlhepp et al. (2011) for Kiruna. In addition, a paper comprising the retrieval settings and errors for many gases, including HCl, $ClONO_2$, and HF, at all NDACC IRWG sites is in preparation at the moment.

Hereafter, some characteristics of the various observation sites are given from north to south. Table 1 lists their coordinates and measurement time periods used in this study. In the Supplement to this publication, the most significant settings for the retrieval of HCl, $ClONO_2$, and HF at each site are described.

2.1 Eureka (80.05° N)

Environment Canada operated a Bomem DA8 FTS at the Eureka NDACC observatory every spring and nearly every fall from 1993 until 2008. Details of this instrument, observations and retrieval methods are given in Fast et al. (2011). In July 2006, the Canadian Network for the Detection of Atmospheric Change (CANDAC) installed a Bruker 125HR FTS in the observatory, now known as the Polar Environment Atmospheric Research Laboratory (PEARL). This instrument makes measurements at $0.0035\,cm^{-1}$ resolution throughout the sunlit parts of the year (mid-February to mid-October). It was run simultaneously with the Bomem DA8 during three campaigns in 2007 and 2008 before the removal of the DA8 in February 2009. Full details of the instrument and retrieval parameters are given in Batchelor et al. (2009). Measurements shown for Eureka in this work include daily average total column densities from the Environment Canada Bomem DA8 between February 1997 and March 2006, and from the CANDAC Bruker 125HR from July 2006 onwards. The biases between the use of the HITRAN 1992 spectral database (for analysis of the DA8 data) and HITRAN 2004 (for analysis of the 125HR data) have been quantified by Fast et al. (2011) based on retrievals from DA8 spectra recorded for one day and for the microwindows indicated for the DA8 in the Tables 1 to 3 of the supplement to the present publication. They are −0.4 % for HCl, +15.6 % for $ClONO_2$, and 0.0 % for HF.

2.2 Ny Ålesund (78.92° N)

At the AWIPEV research base in Ny Ålesund on the Svalbard archipelago, FTIR measurements have been performed since 1990. In the period 1990 to 1995 a Bruker 120M was used. This spectrometer was replaced by a 120HR in 1995. The instruments are operated by the AWI Potsdam and the University of Bremen. Measurements in solar absorption geometry are performed from the end of March until the end of September each year. During polar night, measurements in lunar absorption geometry are performed, which are not used here. The observation range is 600 to 8000 cm^{-1}, depending on the instrument setup, which is changed for the different experiments.

2.3 Thule (76.53° N)

The NDACC FTS stationed at Thule, Greenland, is operated by the National Center for Atmospheric Research (NCAR). The instrument and observing system are described in Hannigan et al. (2009). The instrument is a Bruker 120M FTS that has been blind compared (Goldman et al., 1999) prior to installation at Thule in 1999. The system operates autonomously to record solar absorption spectra in the mid-IR on approx. 30 % of the days between 20 February and 20 October. Observations are taken up to five times per day depending upon weather conditions.

2.4 Kiruna (67.84° N)

Since March 1996, a Bruker IFS 120HR FTIR spectrometer has been operated continuously by the Institute for Meteorology and Climate Research (IMK-ASF) of the Karlsruhe Institute of Technology (KIT, formerly Research Center Karlsruhe) at the Swedish Institute of Space Physics (IRF) in Kiruna, northern Sweden, in collaboration with the IRF Kiruna and the University of Nagoya (Japan). A side-by-side comparison was performed in 1998 with the travelling NDACC standard spectrometer (Meier et al., 2005). The instrument is remotely controlled since July 2004. It was upgraded to a 125HR spectrometer in July 2007. Experimental details have been published elsewhere (e.g. Blumenstock et al., 2006). On average, measurements are taken on about 80 days per year.

2.5 Poker Flat (65.12° N)

The FTS spectrometer, a Bruker 120HR, is located at the Poker Flat Research Range (PFRR) of the Geophysical Institute at the University of Alaska Fairbanks (GI/UAF) under the responsibility of Japan's National Institute of Information and Communications Technology (NICT). The solar absorption spectra used here have been recorded between 1999 and 2004. The FTS automatically records spectra typically on about 100 days per year between February and October. The error analysis for HCl and HF was reported by Kagawa et al. (2007). $ClONO_2$ is not measured operationally at the Poker Flat site and hence no results are reported in this paper.

2.6 Harestua (60.20° N)

Chalmers University of technology has conducted continuous solar FTIR measurements at the Harestua site within NDACC since the end of 1994, with 50–70 measurements per year. The measurement site is a former solar observatory, situated on a hill at 600 m altitude, 50 km north of Oslo. The instrument used is a Bruker 120M spectrometer connected to a solar tracker. Between 1994 and 2004 the original solar tracker of the site was used (coeliostat) but it was later replaced by a custom-built solar tracker allowing remote control of the measurements. The site is frequently located underneath the edge of the polar vortex and the columns measured therefore show a large variability during spring time.

2.7 Zugspitze (47.42° N)

A high-resolution solar absorption infrared sounding system has been operated continuously on the Zugspitze since March 1995 as part of NDACC under the responsibility of the Institute for Meteorology and Climate Research (IMK-IFU) of the Karlsruhe Institute of Technology (KIT). The measurements are performed with a Bruker IFS 125HR interferometer on typically 120–140 days per year. Details have been described by Sussmann and Schäfer (1997).

2.8 Jungfraujoch (46.55° N)

The Jungfraujoch spectra of relevance to the present study have been obtained under the responsibility of the University of Liège, with two FTIR spectrometers, namely a homemade instrument which began routine observations in 1984 and a commercial 120HR model from Bruker, operated since 1990. The measurement density has increased from a yearly average of 50 days between 1985 and 1990 to 114 days from 1991 onwards. The spectral resolution varies between 0.003 and 0.006 cm^{-1}, depending on the species and on the geometry of observation. More details on the instrumentation can be found in Zander et al. (2008). The Jungfraujoch time series used here for HCl and $ClONO_2$ are completely consistent with those of the Rinsland et al. (2003) study; hence the description of the strategies and algorithms used to produce the Jungfraujoch data set given in Appendix A2 of that paper still applies.

2.9 Toronto (43.66° N)

The Toronto Atmospheric Observatory (TAO) was established in 2001 with the installation of a Bomem DA8 FTS. Spectra have been recorded routinely since May 2002. A description of the operations and data analysis can be found in Wiacek et al. (2007). Side-by-side comparisons with two

lower-resolution FTSs were performed in 2005 and are described in Wunch et al. (2007) and Taylor et al. (2008). At present, $ClONO_2$ has not been retrieved at Toronto.

2.10 Tsukuba (36.05° N)

The solar absorption spectra at Tsukuba, Japan were obtained with a Bruker 120M FTS from March 1998 to October 2006 and with a Bruker 120HR FTS since May 2001. The organisations responsible for the analysis of HCl and HF are Tohoku University and the National Institute for Environmental Studies (NIES) in Japan. The spectral fitting algorithm to derive the vertical column densities is based on SFIT1.09e, and is improved with a vertical shift procedure of the initial profile to minimise the residual of the spectral fitting (Murata et al., 2005). In this paper, the data have been derived from the spectra recorded with the Bruker 120M from March 1998 to December 2005 and with the Bruker 120HR from January 2006 to December 2009. Measurement density is 80 days per year on average. $ClONO_2$ has not been retrieved at Tsukuba.

2.11 Kitt Peak (31.90° N)

Measurements of HCl, $ClONO_2$, and HF from Kitt Peak are recorded with the 1-m OPD (optical path difference) FTS (Brault, 1978) in the US National Solar Observatory (NSO) facility in southern Arizona, USA, under the responsibility of NASA Langley Research Center. A five-year gap in observations has occurred, limiting the analysis of the database for the trend in chlorine loading. Limited measurements have restarted in 2009 and have been combined with the previous measurements to produce the total column time series of daily average measurements shown in this paper, with additional measurements anticipated in the near future.

2.12 Izaña (28.30° N)

Since the beginning of 1999, a Bruker IFS 120M FTIR spectrometer has been operated continuously at the Izaña Observatory on Tenerife Island (Schneider et al., 2005). Since 2005, a Bruker 125HR instrument has been used, which was run side-by-side with the 120M spectrometer in April and May 2005. The responsibility for the FTIR experiment lies with IMK-ASF of the Karlsruhe Institute for Technology (KIT). Measurements are taken on about 100 days per year.

2.13 Mauna Loa (19.54° N)

The Mauna Loa Observatory is located on the big island of Hawaii at an altitude of 3.40 km. The observatory is maintained by NOAA's ESRL (Earth Systems Research Laboratory, formerly CMDL, Climate Monitoring and Diagnostics Laboratory). From 1991 to 1995, a Bomem DA8 was located at the site and was replaced by a Bruker 120HR in 1995. FTS data from this site were used in the 1995 Mauna Loa stratospheric ozone inter-comparison (McPeters et al., 1999). The instruments were operated by the University of Denver from 1991 to 2007, and have been operated by NCAR since then (Hannigan et al., 2009). $ClONO_2$ is not retrieved at Mauna Loa due to its low abundance at low latitude.

2.14 La Réunion (21.80° S)

The observing system of the Belgian Institute for Space Aeronomy (BIRA-IASB) at St Denis on Ile de La Réunion is a Bruker IFS 120M spectrometer. Until 2008, this system was deployed at St Denis on a campaign basis; in May 2009, the system was installed for quasi-permanent operation. The data included in the present work come from two measurement campaigns, one in 2004 (August to October) and a second one in 2007 (May to October), and from continuous measurements since May 2009. The instrument and operation characteristics during the 2004 campaign have been described in Senten et al. (2008). In 2007 and 2009, the same instrument was operated in an almost identical way, apart from the fact that the instrument is no longer located in a container on the roof of a university building but in a dedicated laboratory inside the same building. The observations are taken at different spectral resolutions, depending on the solar zenith angle. $ClONO_2$ retrievals have been unsuccessful so far, due to the high humidity at the site and the low $ClONO_2$ abundances at this low latitude.

2.15 Wollongong (34.45° S)

The NDACC site at Wollongong is operated by the local University. It used a Bomem DA8 FTS from 1996 to 2007 (Griffith et al., 1998; Paton-Walsh et al., 2004, 2005). During 2007 the instrument was replaced with a Bruker 125HR FTS. In August 1999, the optical band pass filter that was used to record spectra on the MCT detector was changed from one that transmitted in the 700–1350 cm^{-1} range to two separate filters transmitting in the 700–1050 cm^{-1} and 1000–1350 cm^{-1} ranges.

2.16 Lauder (45.04° S) and Arrival Heights (77.82° S)

The instrument at Arrival Heights was a Bomem from 1991 to 1996 and is since then a Bruker 120M Fourier Transform Spectrometer (FTS), jointly operated by NIWA and the University of Denver, with support from the New Zealand Antarctic Institute. For Lauder, the instrument was an ABB Bomem MB104 in 1986, 1987, and 1989, a Bomem DA2 between 1990 and 1992, a Bruker 120M Fourier Transform Spectrometer until 2001 and a Bruker 120HR from then. Retrievals performed on Lauder data taken between 1986 and 1991 have been analysed with a column scaling algorithm (SFIT1). Fits of the broad absorption of $ClONO_2$ use the technique of pre-fitting interfering gases in a region around the absorption at the 780 cm^{-1} window and then fitting $ClONO_2$ in a smaller microwindow there (Reisinger et al., 1995). HBr cell and ILS measurements (LINEFIT) are

Table 2. Overview of the models. Please note that the vertical domains are pressure altitudes as most models operate on a pressure grid.

Model	Model type	Horizontal resolution	Vertical domain (approx.)	Strat. vertical resolution	Init. year	Bound. cond. (GHG/CFC scenario)	Chemical kinetics
Bremen 2-D model	2-D model	9.5°	0–100 km	∼3.5 km	1958	IPCC (2001) A1B/WMO (2003) Ab	Sander et al. (2006)
KASIMA	CTM	5.6°×5.6° (T21)	7–120 km	∼0.75–3 km	1972	IPCC (2001) A1B/WMO (2003) Ab	Sander et al. (2002)
SLIMCAT	CTM	5.6°×5.6°	0–60 km	∼2 km	1977	IPCC (2001) A1B/WMO (2007) A1	Sander et al. (2002)
EMAC	CCM	2.8°×2.8° (T42)	0–80 km	∼2 km	1958	IPCC (2001) A1B/WMO (2007) A1	Sander et al. (2002)
SOCOL	CCM	3.6°×3.6° (T30)	0–80 km	∼1–5 km	1960	IPCC (2001) A1B/WMO (2003) Ab	Sander et al. (2002, 2006), Atkinson et al. (2004, 2006)

done on a monthly basis at both instrument sites. At Arrival Heights, solar measurements are made from August to March.

3 Models

In addition to the FTIR measurements, results from five different atmospheric models are used in this study, comprising a two-dimensional (2-D) altitude-latitude model similar to the one used in Rinsland et al. (2003), called the Bremen 2-D model, two three-dimensional (3-D) chemistry transport models (CTMs), KASIMA and SLIMCAT, and two 3-D chemistry climate models (CCMs), EMAC and SOCOL (see Table 2). Thereby, the influence of the differing architecture of the models on the trend estimation can be investigated. On the other hand, the two CTMs KASIMA and SLIMCAT can help to estimate the influence of the irregular sampling of the measurements on the trend results (Sect. 5.4). This is possible because those two models use reanalyses calculated from actual measurements so that the state of the atmosphere simulated by the models can be assumed to be as close as possible to reality (please see the specific descriptions below). In contrast, the 2-D model uses only one repeating annual cycle. The two CCMs calculate their own independent and consistent meteorology and dynamics which is not necessarily or rather probably not corresponding to the real meteorological situation.

For the trend calculation and comparison with the FTIR measurements, results from the Bremen 2-D model are used between 2000 and 2008, from EMAC, KASIMA and SLIMCAT between 2000 and 2009, and from SOCOL between 2000 and 2004.

For all five models, the time evolution of the greenhouse gases and ozone-depleting substances was prescribed as a boundary condition at the lower model boundary. The emission scenario for the most important anthropogenic greenhouse gases, i.e. CO_2, CH_4, and N_2O, was the IPCC scenario A1B for all simulations considered here (see also Table 2). It assumes very rapid economic growth, low population growth, and the rapid introduction of new and more efficient technologies (Nakicenovic et al., 2000). The time evolution of the global surface volume mixing ratios of the ozone-depleting substances (ODS) was prescribed according to different so-called baseline scenarios. This means the scenarios represented the best guess for both past and future source gas emissions at the time of their publication. A comparison between them is shown in Fig. 1. KASIMA and the 2-D model applied the Ab scenario from WMO (2003), called REF2 in Fig. 1, while SOCOL used the REF1 modification where updates from newer observations for some source gases were made between 2000 and 2004. The ODS in SLIMCAT and EMAC follow the scenario A1 of WMO (2007). All the ODS data were provided in the framework of the SPARC (Stratospheric Processes And their Role in Climate Change) CCMVal (Chemistry-Climate Model Validation activity) initiative (Eyring et al., 2006, 2007) and were recommended for use as lower boundary conditions in the simulations for the 2006 and 2010 WMO Ozone Assessments.

For the comparison with the FTIR measurements, the model data were interpolated to the locations of the instruments from the adjacent grid points.

3.1 Bremen 2-D model

The 2-D model used in this study is the Leeds-Bremen interactive transport, chemistry and radiation model most recently described by Chipperfield and Feng (2003) and Sinnhuber et al. (2009). It uses the dynamical core of the so-called "two-and-a-half-dimensional" THINAIR model (Kinnersley, 1996) together with the chemistry scheme from the SLIMCAT model (Chipperfield, 1999). The stratospheric dynamics are forced by the amplitudes of waves 1 to 3 of the Montgomery potential at the 380 K isentrope (essentially the same as the amplitudes of the 100 hPa geopotential waves). Here we use the daily Montgomery potential from meteorological analyses with a repeating annual cycle for the period of May 1980 to April 1981. There is no quasi-biennial oscillation (QBO) in the model, i.e. the modelled tropical stratospheric wind is always in a weak easterly state. As we have used no inter-annual variability in the dynamical forcing here, all inter-annual variability comes from changes in

the source gases and aerosol surface area. In this simulation, the following halogen-containing gases are treated explicitly: CFC-11, CFC-12, CFC-113, CCl_4, CH_3CCl_3, Halon-1301, Halon-1211, HCFC-22, and CH_3Cl. In contrast, HCFC-141b is not treated explicitly, but proportionately added to CH_3Cl_3 so that the additional chlorine atoms are accounted for. Analogously, the CFC-114, CFC-115, and HCFC-142b surface mixing ratios are considered in the HCFC-22 value. This model run is the same as used in the 2006 WMO Ozone Assessment (WMO, 2007). Data are available every fifth day until the end of 2008 only.

3.2 KASIMA

The 3-D chemistry transport model KASIMA (Karlsruhe Simulation Model of the Middle Atmosphere) used in this study is a global circulation model including stratospheric chemistry for the simulation of the behaviour of physical and chemical processes in the middle atmosphere (Kouker et al., 1999; Reddmann et al., 2001; Ruhnke et al., 1999). The meteorological component is based on a spectral architecture with the pressure altitude $z = -H\ln(p/p_0)$ as the vertical coordinate, where $H = 7$ km is a constant atmospheric scale height, p is the pressure, and $p_0 = 1013.25$ hPa is a constant reference pressure.

For the present study, the KASIMA version as described in Reddmann et al. (2001) which yields realistic stratospheric age-of-air values (Stiller et al., 2008) was used. The necessary meteorological data of temperature, vorticity and divergence are taken from the European Centre for Medium-Range Weather Forecasts (ECMWF), using ERA-40 data until 2002 and operational ECMWF analyses from 2003 on. In this version, the KASIMA model is relaxed (nudged) toward the ECMWF data between 18 and 48 km pressure altitude using forcing terms with a timescale of 4 h. Below 18 km, the meteorology is based on ECMWF analyses without nudging, and above 48 km pressure altitude, the prognostic model integrating the primitive equations without additional forcing from ECMWF data is used. The model consists of 63 vertical layers between 7 and 120 km and has a horizontal resolution of approximately $5.6° \times 5.6°$(T21).

The photolysis rates are calculated online in KASIMA using the Fast-J2 model of Bian and Prather (2002).

3.3 SLIMCAT

SLIMCAT is an off-line 3-D CTM which has been widely used for the study of stratospheric chemistry (e.g. Feng et al., 2007). The model uses a hybrid $\sigma - \theta$ coordinate (Chipperfield, 2006) and in the stratosphere (θ-level domain), vertical motion is calculated from diagnosed heating rates. This approach gives a reasonable description of the stratospheric circulation and age-of-air (see Monge-Sanz et al., 2007). The model has a detailed description of stratospheric chemistry (see Chipperfield, 1999).

For this study the model was integrated (run 509) from 1977 to 2010 at a horizontal resolution of $5.6° \times 5.6°$ and with 32 levels from the surface to about 60 km. The model was forced using ECMWF reanalyses: ERA-40 from 1977–1988 and then ERA-Interim from 1989–2009. This run did not have an explicit treatment of tropospheric convection but the model assumed that long-lived tracers in the troposphere were well-mixed (see Hossaini et al., 2010).

3.4 EMAC

The chemistry climate model EMAC (ECHAM/MESSy Atmospheric Chemistry model) has been developed at the Max-Planck-Institute for Chemistry in Mainz (Jöckel et al., 2006). It is a combination of the general circulation model (GCM) ECHAM5 (Roeckner et al., 2006) with different submodels, for example the chemistry submodel MECCA (Module Efficiently Calculating the Chemistry of the Atmosphere) (Sander et al., 2005) linked by the Modular Earth Submodel System (MESSy) interface (Jöckel et al., 2005). The simulation performed here includes a comprehensive stratospheric chemistry. The volcanic stratospheric aerosols and the solar irradiance were constant, the QBO was not included and additional bromine with respect to the very short-lived substances (VSLS) was not added. Sea surface temperature (SST) and sea ice cover (SIC) datasets have been used from one of the IPCC-AR4 ECHAM5/MPI-OM coupled model A1B scenario runs performed for the IPCC Fourth Assessment Report (IPCC, 2007).

3.5 SOCOL

The SOCOL_v2.0 (SOlar Climate Ozone Links Version 2) CCM combines the MAECHAM4 GCM (Manzini et al., 1997) with the CTM Mezon (Egorova et al., 2003). SOCOL contains a comprehensive stratospheric chemistry scheme consisting of 41 chemical species, 118 gas-phase reactions, 33 photolysis reactions and 16 heterogeneous reactions (Egorova et al., 2005; Schraner et al., 2008). Inorganic fluorine species (e.g. HF) are not simulated. The Cl_y member species (HCl, $ClONO_2$, HOCl, OClO, Cl, ClO, Cl_2O_2) are individually transported, while the 14 organic-chlorine-containing species present in the model are grouped into two families (short- and long-lived) and these two families are then explicitly advected. After each transport step, the individual members of the two families are partitioned before the chemical computations. 13 photolytic, 14 $O(^1D)$ and 8 OH reactions are used to model the photochemical breakup of the 14 organic-chlorine-containing species. Implications of employing such a scheme are investigated in Struthers et al. (2009).

The model data used in this study originate from the NIWA-SOCOL REF-B1 simulation performed for the WMO SPARC CCMVal2 activity (Eyring et al., 2008). Boundary conditions and model parameters used in the REF-B1

Table 3. Mean differences between models and FTIR measurements in % (calculated as (model-meas)/meas) averaged over all sites, and their standard deviations, for HCl, $ClONO_2$, and HF. The differences for KASIMA and SLIMCAT were calculated from the daily values, while for EMAC, SOCOL, and the 2-D model, the monthly means were used.

gas	KASIMA	SLIMCAT	2-D model	EMAC	SOCOL
HCl	-11.90 ± 8.58	$+10.48 \pm 7.92$	$+8.32 \pm 15.93$	-24.84 ± 8.08	$+9.49 \pm 13.83$
$ClONO_2$	$+11.57 \pm 58.33$	$+90.00 \pm 146.78$	$+15.40 \pm 41.13$	$+30.10 \pm 90.59$	-17.31 ± 22.96
HF	$+1.79 \pm 10.44$	$+36.25 \pm 12.72$	-14.28 ± 12.63		

CCMVal2 simulations are described in Morgenstern et al. (2010). The data available here are monthly means until the end of 2004 only.

4 Time series

Before calculating and comparing the HCl, $ClONO_2$, and HF trends, the consistency of the total column abundances between the FTIR measurements and the different models is investigated (Figs. 3 to 5). Table 3 shows the mean relative differences between each model and the measurements, averaged over all sites. The differences for the CTMs KASIMA and SLIMCAT were calculated from the daily means of the FTIR measurements and the 12:00 UTC model output because these two models use meteorological analyses as boundary conditions so that every day's atmospheric state should be comparable. In contrast, for the CCMs EMAC and SOCOL and the 2-D model, the monthly means from models and measurements were used for the comparison because these models calculate their own dynamics and meteorology which do not necessarily correspond to the real situation on each day. The normalised mean monthly mean values determined for 2000 to 2009 (Figs. 6 to 8) allow us to investigate the characteristics of the seasonal cycle of each gas and its amplitude. These mean monthly means were calculated by dividing the monthly means by the corresponding annual mean and then averaging each month over the whole time period 2000–2009. In all three gases, a seasonal cycle is expected that is connected with the seasonal variation of the tropopause height. This variation results from the stratospheric general circulation transporting air from the summer to the winter hemisphere. The higher the tropopause, the smaller is the relative contribution of the stratosphere to the total column abundance. This again results in a lower total column abundance of HCl, $ClONO_2$, and HF in summer, because they are all mainly produced in the stratosphere. In the high latitude regions, HCl and $ClONO_2$ are in addition influenced by the absence of solar irradiation in winter. Chlorine activation on the surface of polar stratospheric clouds (PSCs) leads to a decrease in the total column abundances of the chlorine reservoir species and a strong peak at the end of the winter due to the deactivation of active chlorine. So the seasonal cycle is expected to exhibit its largest amplitude at the polar sites.

4.1 HCl

Measurements and models both indicate a steady increase of HCl until about the mid-1990s. Afterwards, a decrease of the HCl total column abundances is observed at all sites, with the Southern Hemisphere delayed by a few years with respect to the Northern Hemisphere (Fig. 3).

In comparison to the FTIR measurements, KASIMA underestimates the total column abundances of HCl (Fig. 3 and Table 3). Reasons for this are discussed in Kohlhepp et al. (2011, and references therein) and include the horizontal resolution, the data set used for nudging, and the parameterisation of tropospheric processes, for example. In contrast, the other CTM, SLIMCAT, tends to overestimate the total HCl content compared to the measurements. The average bias is smallest for the 2-D model (Table 3). EMAC underestimates the HCl total column even more than KASIMA, while SOCOL overestimates it.

In the FTIR data, the annual maximum of HCl occurs in spring, around April/May in the Northern Hemisphere and October/November in the Southern Hemisphere (Fig. 6). This seasonal cycle is qualitatively captured at most sites by all models except the 2-D one. At some sites, KASIMA and SOCOL simulate the annual maximum about one month too early.

4.2 $ClONO_2$

Because of its weak spectral signature, interference by water vapour, and the low column abundances especially at lower latitudes, $ClONO_2$ is not easy to measure with a ground-based FTIR spectrometer. For this reason there are no $ClONO_2$ time series from the FTIR sites Poker Flat, Toronto, Tsukuba, Mauna Loa, and La Réunion which are therefore not included in the comparisons in Figs. 4 and 7 and Table 3.

All measurement and model datasets show an increase of $ClONO_2$ until the late 1990s and a decrease afterwards (Fig. 4).

At the Northern Hemisphere high latitude sites Ny Ålesund, Thule, and Kiruna, the models tend to overestimate the total atmospheric $ClONO_2$ content, especially the annual minima (Fig. 4). At most sites, the SLIMCAT model shows the highest values, followed by EMAC and the 2-D model. On average, KASIMA, SOCOL, and the 2-D model agree best with the measurements (Table 3).

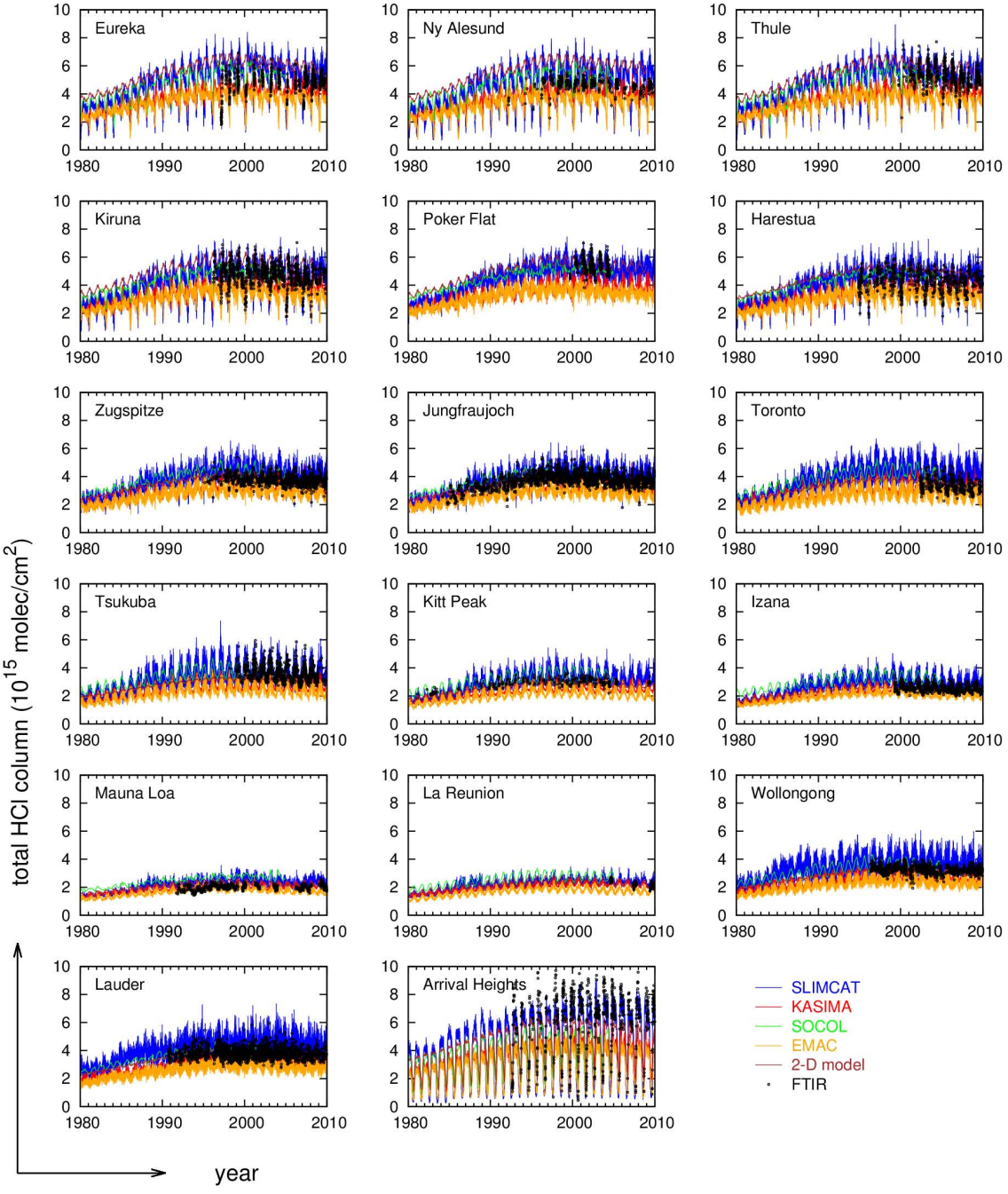

Fig. 3. Time series of HCl total column abundances in molecules per cm^2 at the different sites as measured by FTIR (black dots) and simulated by SLIMCAT (blue line), KASIMA (red line), SOCOL (green line), EMAC (orange line), and Bremen 2-D model (brown line).

SLIMCAT simulates a stronger relative seasonal variation than the other models at most Northern Hemisphere sites (Fig. 7). At midlatitudes, this means SLIMCAT overestimates the $ClONO_2$ amplitude, while closer to the poles, the other models tend to underestimate it. The annual $ClONO_2$ maximum occurring in February or March at most Northern Hemisphere sites is captured qualitatively by most models. Especially in the Northern Hemisphere midlatitudes, EMAC tends to simulate the maximum in April, which is about one month later than the other models which agree with the measurements. At the Southern Hemisphere sites Wollongong and Lauder, the maximum predicted by the models between August and October is not very pronounced in the measurements.

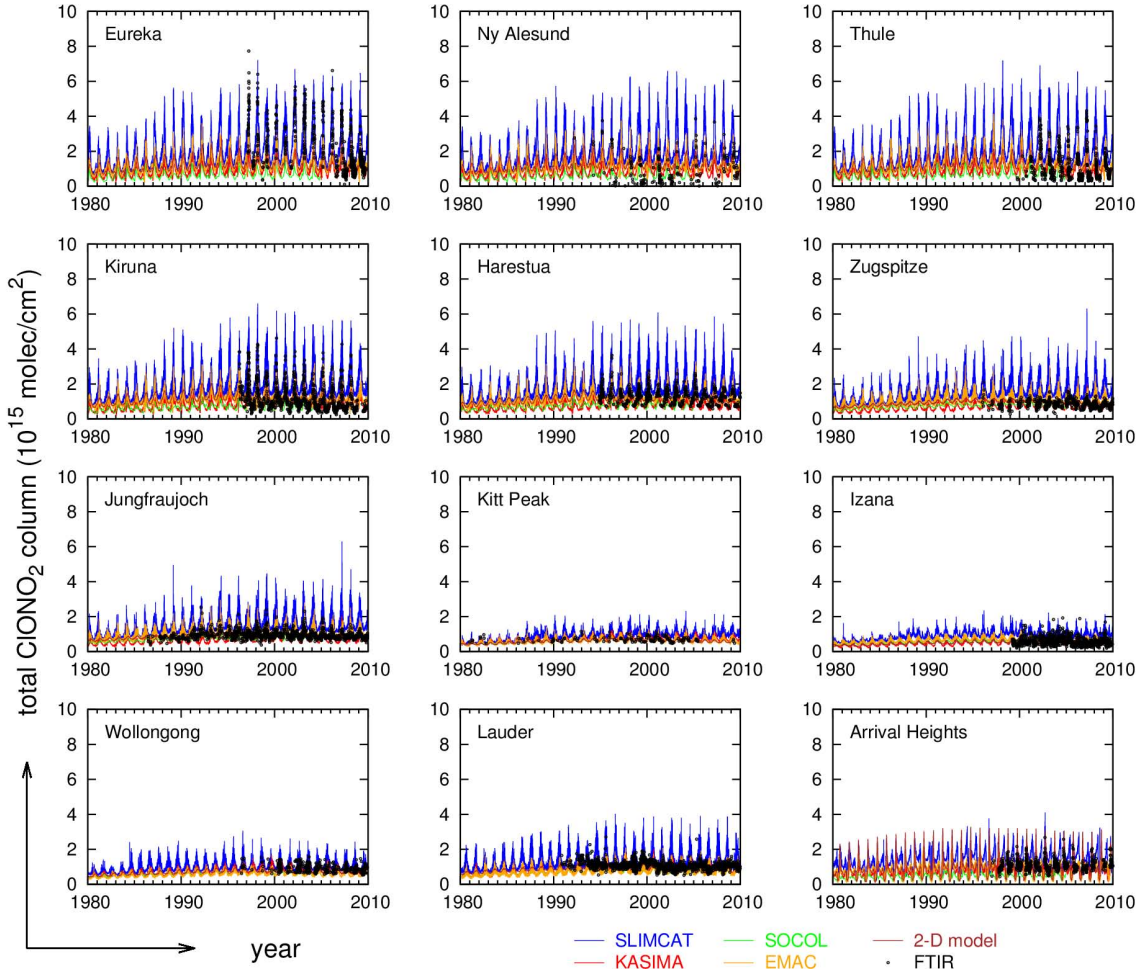

Fig. 4. Time series of $ClONO_2$ total column abundances in molecules per cm^2 at the different sites as measured by FTIR (black dots) and simulated by SLIMCAT (blue line), KASIMA (red line), SOCOL (green line), EMAC (orange line), and Bremen 2-D model (brown line).

4.3 HF

The two CCMs EMAC and SOCOL do not simulate the atmospheric HF content, therefore only the results from the CTMs KASIMA and SLIMCAT and from the 2-D model can be compared with the FTIR measurements at the 17 sites. They show an increase over the largest part of the time range that weakens in the last few years (Fig. 5).

The SLIMCAT model tends to overestimate the HF total column abundance, while KASIMA on average agrees better with the measurements. The 2-D model shows a behaviour very similar to KASIMA apart from some low and midlatitude sites (e.g. Toronto, Kitt Peak, Izaña, and La Réunion) where it tends to underestimate the increase especially in the 1990s (Fig. 5). This results in a mean underestimation of the measured total column abundances by the 2-D model (Table 3).

The amplitude of the seasonal HF cycle as simulated by the two CTMs KASIMA and SLIMCAT fits very well to the one measured by the FTIR spectrometer at most sites (Fig. 8). The annual maximum around March and April in the Northern Hemisphere and in October in the Southern Hemisphere is also represented in the two models. The seasonal cycle from the 2-D model is very similar to those from KASIMA and SLIMCAT in the northern polar latitudes, but its amplitude is mostly too weak, especially at the Northern Hemisphere midlatitude sites.

4.4 Summary of the time series comparison

In summary, there is good overall agreement between the FTIR measurements and the models considered here concerning the increase of the total column abundances of HCl and $ClONO_2$ until about the mid-1990s, a decrease afterwards, and on a HF increase that slowly reached a plateau in the last few years. Also the mean annual cycles derived from the different datasets are similar.

The SLIMCAT model tends to overestimate the atmospheric content of the three gases and, especially at midlatitudes, the amplitude of the seasonal cycle of $ClONO_2$.

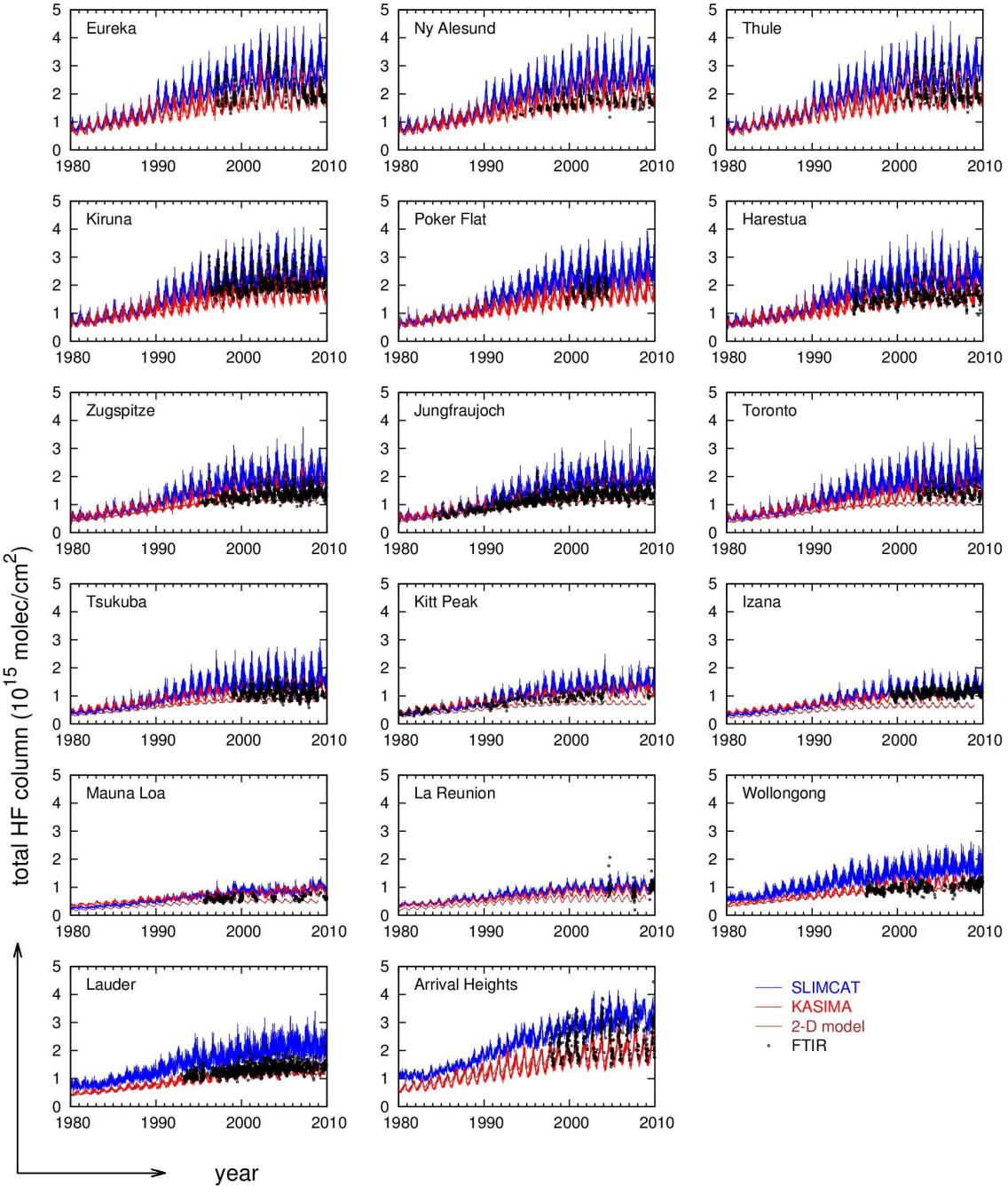

Fig. 5. Time series of HF total column abundances in molecules per cm^2 at the different sites as measured by FTIR (black dots) and simulated by SLIMCAT (blue line), KASIMA (red line), and Bremen 2-D model (brown line).

KASIMA and EMAC tend to underestimate the HCl total column abundance, while SOCOL and the Bremen 2-D model overestimate it, especially in the Northern Hemisphere. The 2-D model underestimates the HF increase at some low and midlatitude sites.

5 Trend method and sensitivity studies

In this section, a short description of the trend calculation method is given, especially also of the bootstrap method used to estimate the trend uncertainty. In addition, we investigate the dependence of the trend result on the type of fit function, the time period, and on sampling. The first two influencing factors are analysed using the FTIR measurements, while

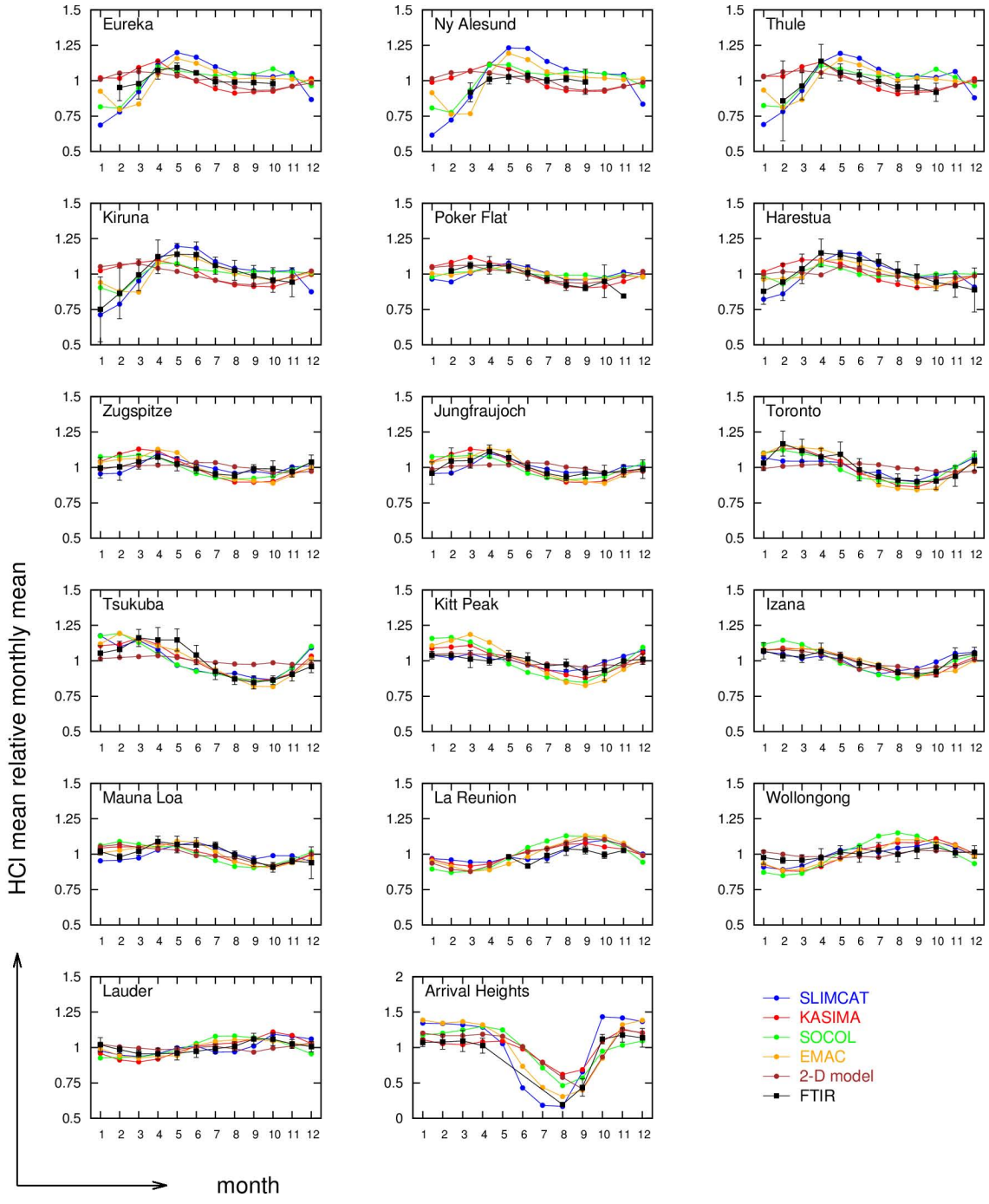

Fig. 6. Annual cycle of HCl at the different sites as determined from the FTIR instruments (black) and simulated by SLIMCAT (blue), KASIMA (red), SOCOL (green), EMAC (orange), and the Bremen 2-D model (brown). The mean relative monthly means were calculated by normalising the monthly means with the respective annual mean and then averaging over the period 2000–2009. The error bars of the FTIR measurements represent the standard deviation.

the sampling influence can be estimated with the help of the CTM data. The main time period chosen for the trend and its sensitivity investigations is 2000–2009. This was done because a continuous decrease is expected for the chlorine gases and an increase for HF during this time so that a linear trend fit can be assumed to sufficiently represent the temporal evolution of the total column abundances. Moreover, nearly all sites included in this study measured during this time (see Table 1).

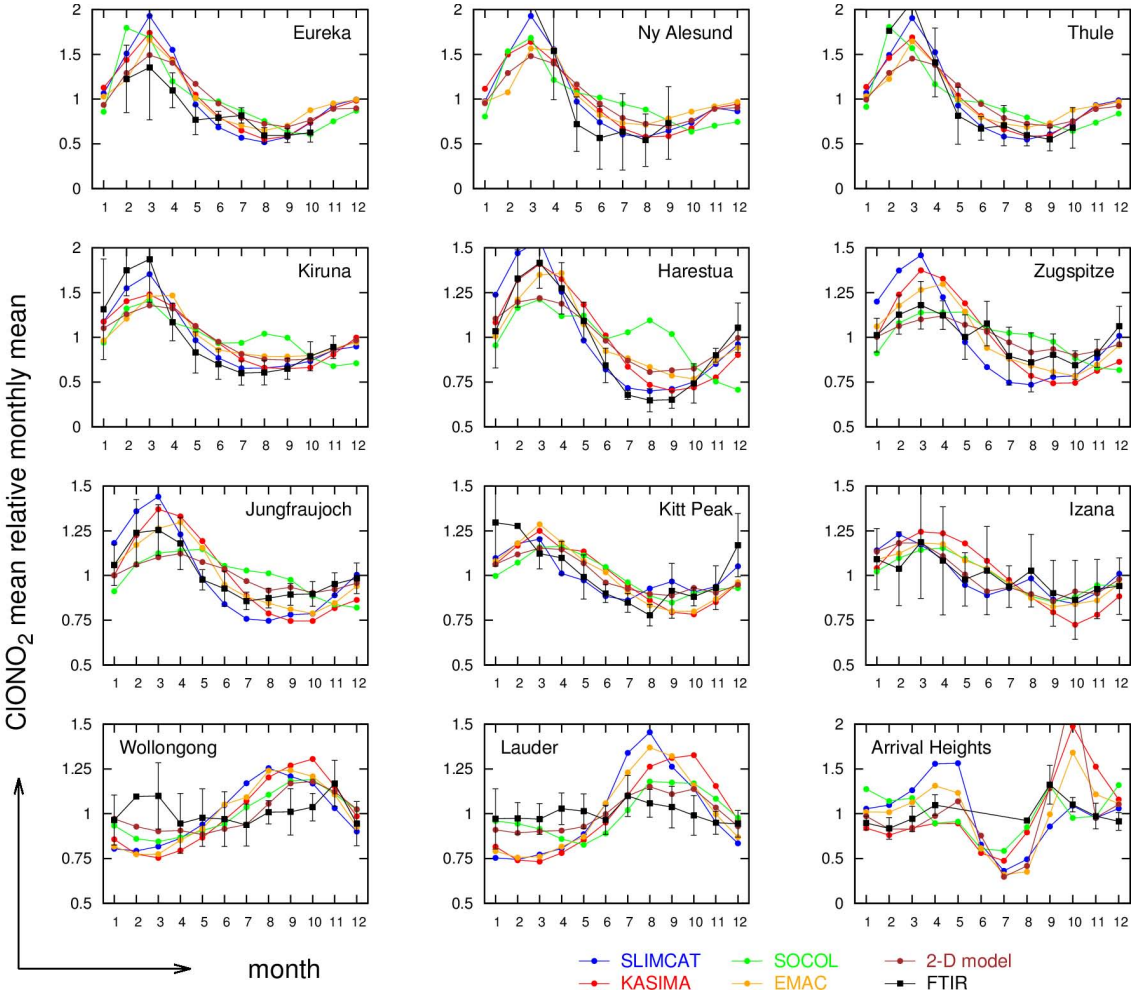

Fig. 7. Annual cycle of $ClONO_2$ at the different sites as determined from the FTIR instruments (black) and simulated by SLIMCAT (blue), KASIMA (red), SOCOL (green), EMAC (orange), and the Bremen 2-D model (brown). The mean relative monthly means were calculated by normalising the monthly means with the respective annual mean and then averaging over the period 2000–2009. The error bars of the FTIR measurements represent the standard deviation.

5.1 Trend determination method

A linear trend function, combined with a Fourier series accounting for the seasonal cycle, is fitted to the time series using a least squares method. The precision of the fit parameters and thus of the trend is determined with the bootstrap resampling method. This method is only described shortly here, however, more detailed information can be found for example in Gardiner et al. (2008, and references therein). It has been used in previous trend studies from FTIR measurements (e.g., Gardiner et al., 2008; Mikuteit, 2008; Vigouroux et al., 2008; Kohlhepp et al., 2011). From the main fit to the data, the differences between fit and data are calculated. These residuals are then added randomly (with replacement) to the fit result in order to create a new, artificial data set. Another fit using the same function as for the real data is performed on the artificial data set, giving an artificial value for every parameter, including the trend. This procedure is applied 5000 times in this study, following the example of Gardiner et al. (2008). From the 97.5 and 2.5 percentiles of the resulting 5001 trend values, the 95 % confidence interval characterising the trend uncertainty can be estimated. The reason for choosing this method to determine the trend uncertainty is that it does not assume that the residuals of the fit to the data are normally distributed. Instead, it only assumes that there are enough data points for the residuals to sufficiently represent their own distribution. The assumption of a normal (Gaussian) distribution of the residuals might not be valid because the fit is not always able to capture the complete annual cycle, e.g. the strong peak in $ClONO_2$ at the polar sites in spring. The main reason for this is that the peak does not always occur at exactly the same time of year.

At all sites between 70° S and 70° N except La Réunion, a third order Fourier series is used to account for the seasonal

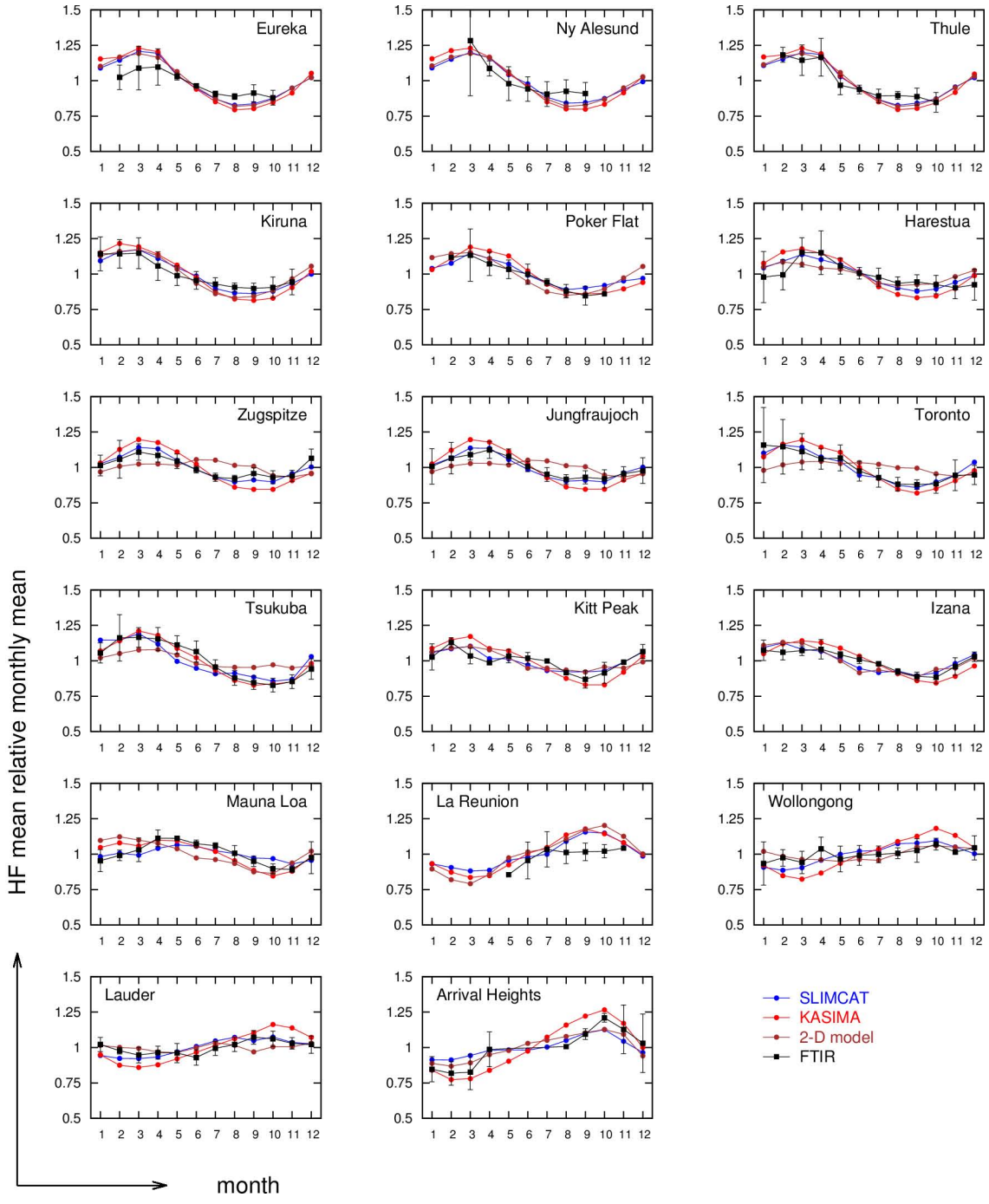

Fig. 8. Annual cycle of HF at the different sites as determined from the FTIR instruments (black) and simulated by SLIMCAT (blue), KASIMA (red), and the Bremen 2-D model (brown). The mean relative monthly means were calculated by normalising the monthly means with the respective annual mean and then averaging over the period 2000–2009. The error bars of the FTIR measurements represent the standard deviation.

cycle. As also found by Gardiner et al. (2008), this approach represents most time series very well and at the same time avoids over-fitting the data. But at the sites poleward of 70° N and S, the FTIR measurements are limited by polar night so that the comparably strong seasonal cycle is only partly represented in the time series. Similarly, a large part of the seasonal cycle is missing also in the La Réunion data where the measurements were performed on a campaign basis. This is why at these sites, for some of the gases, the bootstrap method together with the third order Fourier series fit did not

produce reliable results. So finally, only a first order Fourier series was fitted for all gases measured at these sites in order to account at least for some seasonal variation.

All trend values in this paper are given in % per year referring to the linear fit value computed for 1 January 2000, 12:00 UTC.

For HCl and HF, results for all 17 sites are presented, while for $ClONO_2$, only 12 time series are available (see Table 1). Please note that the measurements at Poker Flat ended in 2004.

5.2 Dependence on the trend calculation approach

In order to estimate the dependence on the type of fit function used, the trends between 2000 and 2009 were determined by fitting a linear function only (this approach is called "linear" from now on) and a linear function combined with a third or first (see above) order Fourier series (called "standard") to the FTIR measurements (Fig. 9). Trends were also calculated by considering the summer and autumn data separately (June to November and December to May in the Northern and Southern Hemisphere, respectively), which are assumed to show less variability, using a simple linear fit function. This method is called "summer/autumn" or "s/a" from now on.

At Toronto and La Réunion, the measurements were started after the year 2000, in 2002 and 2004, respectively. For Toronto, the dependence on the trend calculation approach was determined for the time range 2002–2009, while La Réunion was not considered in this section. There are no results for $ClONO_2$ at Ny Ålesund displayed in Fig. 9. For the summer/autumn series at this site, the bootstrap method did not produce reliable results, and both the linear and the standard procedures led to trend values (10.9 and 6.8 % yr^{-1}, respectively) much higher than at the other sites so that for clarity of the majority of the results, the y-range used here was adapted to them. Analogously, the trend for $ClONO_2$ at Eureka from the linear fit function cannot be displayed (-7.2 % yr^{-1}), and neither the linear HF trend at Poker Flat (3.1 % yr^{-1}).

The confidence interval determined with the bootstrap method is obviously larger for the linear trend alone and the summer/autumn data only than when a linear function combined with a Fourier series is fitted to all data (Fig. 9). This suggests that the linear function alone does not sufficiently represent the time series. Also, the time series restricted to the summer/autumn data naturally contain fewer measurements which is probably the reason for the large error bars noted in these cases.

The results for HCl from the different trend calculation approaches agree within their errors at all sites. For $ClONO_2$, the error bars are larger than those for HCl at most sites. This can be explained partly by the larger amplitude of the seasonal cycle of $ClONO_2$ which cannot be completely represented by the fitting function. In addition, $ClONO_2$ is

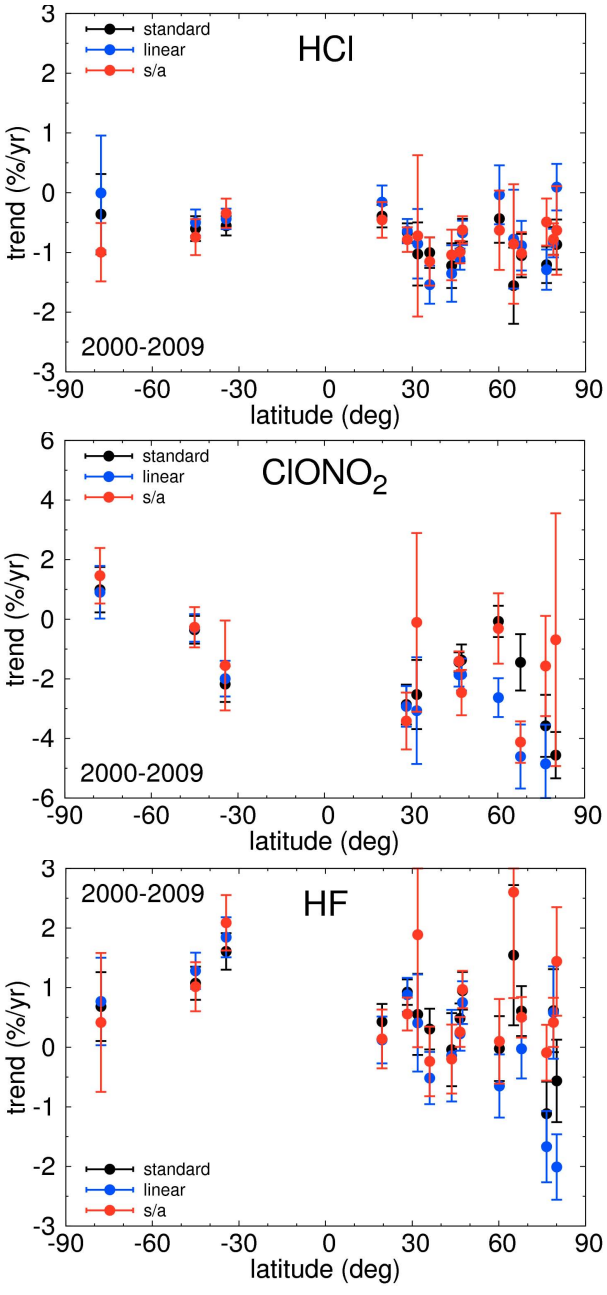

Fig. 9. Dependence of the resulting trend (in % per year) on the type of fitting function, determined from the FTIR measurements of HCl (top), $ClONO_2$ (mid), and HF (bottom) for the time range 2000–2009 (except at Toronto where it is 2002–2009, and at Poker Flat it is 2000–2004). Please note the different y-scales. The results of the "standard" procedure using a linear function with a third or first order Fourier series are shown in black, those of the "linear" trend calculation in blue and of the linear calculation with summer/autumn data only ("s/a") in red. The error bars were determined with the bootstrap method. Concerning the reasons for missing trend values please see text.

difficult to measure and therefore the scatter characterising the total column time series is larger, too. Apart from Eureka, Kiruna, and Harestua, the trend results for $ClONO_2$ from the different approaches agree within errors. The HF trends also agree within errors except at the polar sites Eureka, Thule, and Poker Flat.

There are a few possible reasons for the disagreement of the different trend determination methods at some of the high latitude sites. Due to the influence of the polar vortex, the amplitude of the seasonal cycle is very large and therefore especially the result from fitting the linear function alone very much depends on the start and end time of year. But also the Fourier series cannot capture the sometimes strong variations on a short timescale resulting from the movement of the polar vortex. In addition, the high-latitude seasonal cycles are not completely represented in the time series because solar FTIR measurements are not possible during polar night. Furthermore, at some sites, the time series contain very few data points for the summer/autumn months, for example the $ClONO_2$ series from Ny Ålesund and Wollongong, and all three series from Kitt Peak. At Eureka, the DA8 measurements were performed on a (spring and autumn) campaign basis so that until the installation of the 125HR spectrometer in 2006, there were years with no measurements during "summer/autumn" at all.

5.3 Dependence on the time period used

In order to investigate the influence of time series length and the time period chosen, the FTIR trends were calculated for the three periods 1996–2009, 2000–2009 and 2004–2009 (Fig. 10). The longest period was selected because not all, but more than half of the stations performed measurements during this time, while only a few did before. The longer the time series, the smaller the error bars and the better the trend estimate is expected to be. During the second period, all sites except La Réunion and Toronto performed measurements (see below). From earlier studies, e.g. the one by Rinsland et al. (2003), we expect the inorganic chlorine species total column abundances to have reached their plateau around 1996–1999 and not to strongly change during this time. So the decrease expected due to the Montreal Protocol may be weaker if these four additional years are included in the trend calculation. The latest and shortest period was included in this study in order to investigate whether there was a change in the rate of increase (of HF) or decrease (of HCl and $ClONO_2$) during the last few years.

The approach called "standard" here was used, which means the fitting function was the linear one with a third or first order Fourier series (see above) representing the seasonal cycle. The sites where the required time ranges were not available were not considered in this comparison, except for Toronto, where the trend with the 2000–2009 colour actually covers the time range between 2002 and 2009. There are no trend results for Poker Flat between 2004 and 2009

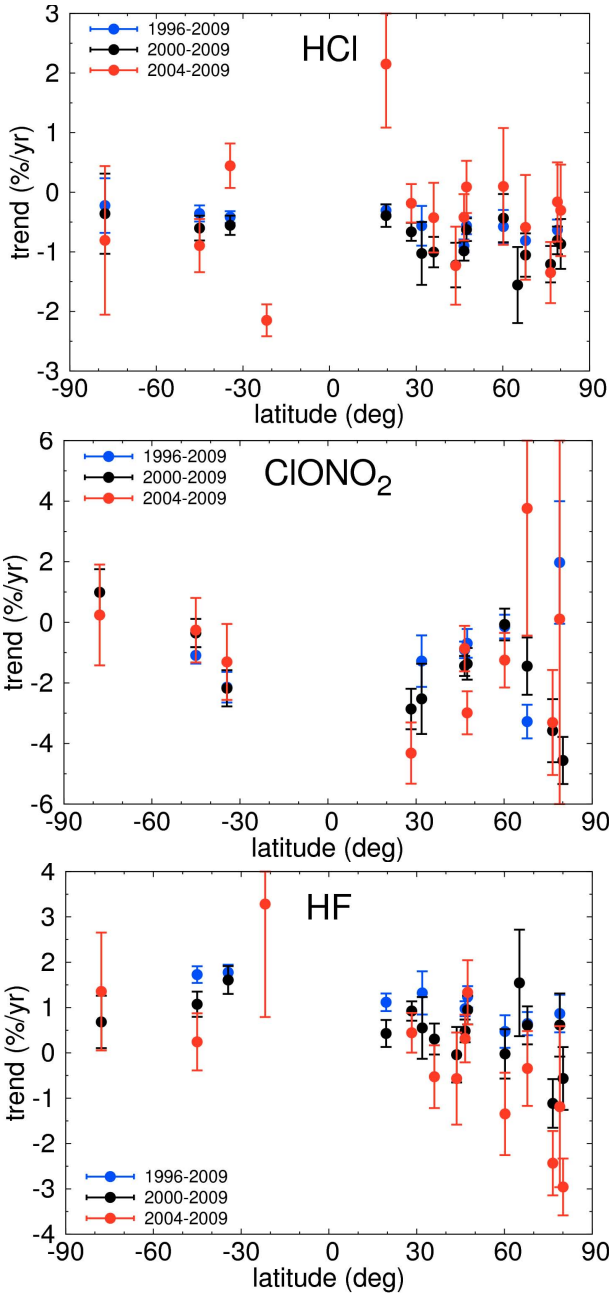

Fig. 10. Dependence of the resulting trend (in % per year) on the time period, determined for the FTIR measurements of HCl (top), $ClONO_2$ (mid), and HF (bottom). Please note the different y-scales. The fitting function is the linear one with seasonal cycle, which is called "standard" here. The results for 1996–2009 are shown in blue, those for 2000–2009 in black (at Toronto, this is 2002–2009, and at Poker Flat it is 2000–2004) and for the 2004–2009 period in red. The error bars were determined with the bootstrap method. Concerning the reasons for missing trend values please see text.

because the time series end in 2004 (see Table 1). In the Kitt Peak data, there is a large gap around 2006 to 2008 so that especially the determination of the seasonal cycle between 2004 and 2009 is not possible and the 2004–2009 trends at this site could not be included either. In the $ClONO_2$ picture of Fig. 10, the trends for Eureka between 2004 and 2009 and for Ny Ålesund between 2000 and 2009 are missing because they are larger than the y-scale (-6.2 and $6.8\,\%\,yr^{-1}$, respectively). The same is the case for the Wollongong and Mauna Loa HF trends between 2004 and 2009: they amount to 4.2 and $22.8\,\%\,yr^{-1}$, respectively.

The shorter the time series, the larger the error bar of the trend (Fig. 10).

In the Northern Hemisphere mid and low latitudes, the HCl trends tend to be less strongly negative for the period from 2004 to 2009 than for the two longer periods, but strongest for 2000 to 2009 at most sites. It must be considered that six years are not enough to reliably determine such small trends (see also Weatherhead et al., 1998). In the Southern Hemisphere, no clear signal is detectable.

For HCl and $ClONO_2$, the trends from 1996 to 2009 and 2000 to 2009 agree within errors at most sites. The expected tendency of a weaker decrease in the chlorine species during 1996–2009 that was discussed above can indeed be found in the presented results, especially for HCl. It is probably due to the stratospheric chlorine loading reaching a plateau at the end of the 1990s and only then slowly starting to decrease.

The reason for the HF trend differing for the three time periods at most sites is probably that the column abundances seem to have reached a plateau in the last few years (see also Fig. 5). The trend is strongest and mostly positive for the longest period, while for the later and shorter periods it weakens or even becomes negative, especially in the Northern Hemisphere.

5.4 Influence of sampling

Due to varying weather conditions at all sites, polar night and midnight sun, and instrumental failures, the sampling of the FTIR data points is not regular and some time series contain gaps. The sampling influence on the trend can be investigated with the chemistry transport models KASIMA and SLIMCAT. As they use meteorological analyses to calculate the atmospheric chemistry processes and transport, the meteorological conditions are assumed to be as close as possible to reality. Therefore, two different model trends for HCl, $ClONO_2$, and HF have been determined by fitting a linear function with a third or first order Fourier series to the CTM data: one from the complete CTM time series containing one value per day and the other one only from the days where FTIR measurements have been taken. The period chosen for this comparison is again 2000–2009. This means La Réunion is not included and the trend calculations for Toronto all start in 2002, while for Poker Flat, they end in 2004, like in Sect. 5.2.

In Fig. 11, the KASIMA (left column) and SLIMCAT (right column) trends from the complete time series are compared with those from the measurement days only and with the FTIR results. It is obvious that there are differences in the trends between the differently sampled time series for both models. At the same time, it is not easy to quantify this sampling influence. However, at most sites, the influence is not very strong so that the trends agree within their bootstrap error bars. The locations where this is not the case are mostly high latitude sites where due to polar night a large portion of the relatively strong annual cycle is missing in the measurement time series, or other sites with large measurement interruptions. At such sites, the error induced by sampling is obviously not negligible.

5.5 Summary of the FTIR trend dependencies

Especially at locations where the seasonal cycle of the gas investigated has a large amplitude, the trend results depend on whether the Fourier series is included in the fit function or not (Sect. 5.2). The linear function alone clearly cannot sufficiently represent the time series. Selecting only the summer/autumn data where the variability is expected to be small does not strongly diminish the confidence intervals. Probable reasons for this are that at some sites, there are not many data points left when removing those measured in winter and spring, and that there is still some variability left in the summer/autumn time series.

When calculating trends for different parts of the time series, the shorter the time series, the larger the error bars (Sect. 5.3). The results for the six-year period 2004 to 2009 should be treated cautiously. Still, there is a considerable tendency towards a decrease of the positive HF trend in the last few years at many Northern Hemisphere measurement sites.

Moreover, as shown in Sect. 5.4, a considerable bias may be induced in the trend results at sites with very irregular sampling or large gaps in the time series. This must be kept in mind when trends from FTIR data are compared with those from model calculations.

It can be concluded that, overall, the agreement between the different trend determination approaches and the different time ranges is good. This means the results are robust. For the trend determination from models and measurements in the following (Sect. 6), the so-called standard approach fitting a linear trend with a Fourier series is used because its error bars are the smallest. The best time period to determine the trends would of course be the longest one (1996–2009), but because many sites started measuring after 1996, in order to ease the comparison or rather to be able to consider more sites, the period chosen for the model-measurement comparison is 2000–2009.

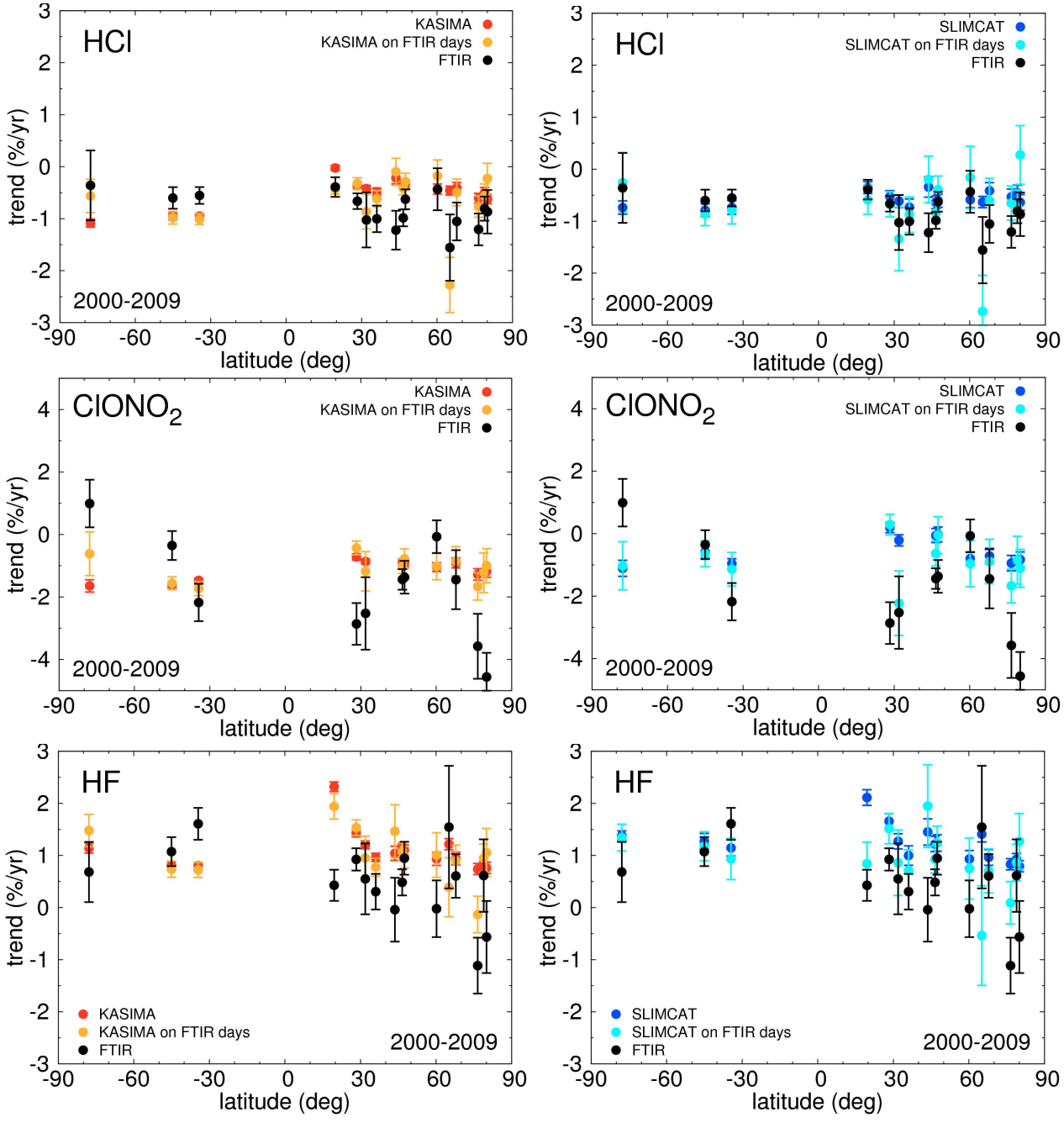

Fig. 11. The dependence of the resulting trend (in % per year) on sampling is investigated by comparing trends from the KASIMA data on all days (left column; red) with those calculated from the model time series on days with FTIR measurements only (orange) and with the FTIR trends themselves (black). The same comparison is shown for SLIMCAT (right column; blue) and SLIMCAT only on FTIR days (cyan). Please note the different y-scales. The error bars were determined with the bootstrap method.

6 Comparison of FTIR and model trends

In this section, the trends from the FTIR measurements are compared with the results from all five models SLIMCAT, KASIMA, SOCOL, EMAC and the 2-D model (see Fig. 12 and Tables 4 to 6). For all models, the trends were determined from all available data, which is one value per day for KASIMA, SLIMCAT, and EMAC, one every fifth day for the Bremen 2-D model, and monthly means for SOCOL. Still, the investigations of Sect. 5.4 have to be kept in mind, showing an influence of the FTIR sampling on the trend results. The period considered here is 2000 to 2009 and the

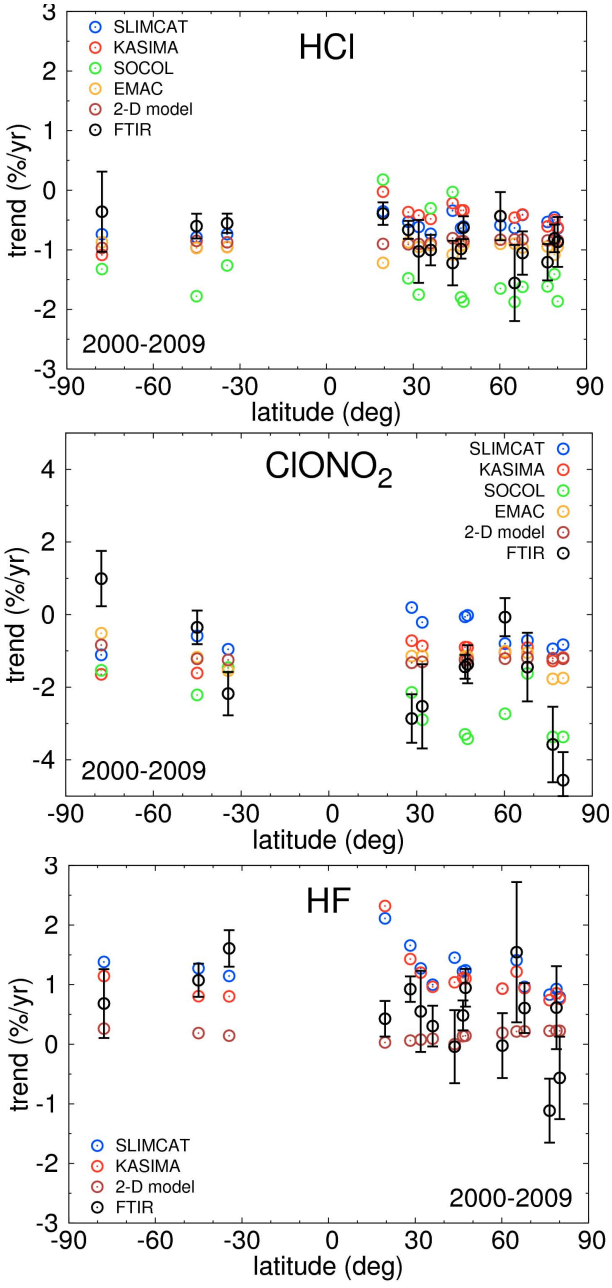

Fig. 12. Comparison of the trends from the FTIR measurements (black) between 2000 and 2009 (in % per year) with those modelled by SLIMCAT (blue), KASIMA (red), SOCOL (green), EMAC (orange), and the Bremen 2-D model (brown) for HCl, $ClONO_2$, and HF. In order not to overload the picture, the bootstrap error bars for the modelled trends are not shown, only those for the measurements. Concerning the reasons for missing trend values please see text.

fit function the linear one with seasonal cycle, following the conclusions of Sect. 5.5.

Concerning SOCOL, it must be remembered that the model time series end in 2004 so that the trends are only determined from a five-year period. Therefore, the trends should not be interpreted quantitatively, but they might qualitatively reproduce the measured signal.

6.1 HCl

In the Northern Hemisphere mid and high latitudes, all models except SOCOL underestimate the decrease of HCl, while in the Southern Hemisphere, they tend to overestimate it (Fig. 12, Table 4). This is mostly due to the FTIR trends indicating a stronger decrease in the Northern Hemisphere than in the Southern Hemisphere and most models not showing a difference between the hemispheres at all. The only model simulating slightly different trends is KASIMA, but its signal is opposite to the FTIR one with relatively stronger negative trends at the Southern Hemisphere sites. SOCOL overestimates the decreasing trend in the mid and high latitudes in both hemispheres but underestimates it at some sites in the Northern Hemisphere tropics. The tendency towards a relatively weaker decrease in the lower latitudes than everywhere else can also be found in KASIMA and SLIMCAT and corresponds to the results from the measurements. EMAC shows the opposite signal and the 2-D model none.

6.2 $ClONO_2$

The $ClONO_2$ trends of models and measurements do not agree as well as the HCl results and also show stronger latitudinal dependencies (Fig. 12, Table 5). In the Northern Hemisphere, all models except SOCOL underestimate the relative decrease seen in the FTIR measurements, as for HCl. The FTIR trends are stronger in polar and low latitudes than in the midlatitudes. An increasingly negative trend towards the north pole can also be seen in all models apart from the 2-D model. One should keep in mind that the measured Eureka $ClONO_2$ trends might be influenced by the bias between the two different line lists used, which is described in Sect. 2.1. In the Southern Hemisphere, for Wollongong the models underestimate the decrease seen in the measurements, while above Lauder, the FTIR trend is weaker than the models simulate. The measured $ClONO_2$ trend is positive above Arrival Heights and becomes increasingly negative towards lower latitudes. The EMAC results behave qualitatively similar there, while the other models show no clear signal.

6.3 HF

Of the three models which actually simulate HF, the 2-D model shows the weakest increase, which does not vary strongly with latitude (Fig. 12, Table 6). KASIMA and SLIMCAT agree well on a positive trend at all sites, with the highest values in the Northern Hemisphere low latitudes, at Mauna Loa and Izaña. In the Southern Hemisphere, none of the models shows a distinct latitudinal dependency, while the FTIR results suggest that the increase weakens towards

Table 4. HCl trend in % per year between 2000 and 2009, calculated by fitting a linear function combined with a first (sites poleward of 70°) or third order Fourier series to the data. The error bars were determined with the bootstrap method.

Measurement site	FTIR	KASIMA	SLIMCAT	2-D model	EMAC	SOCOL
Eureka	-0.87 ± 0.42	-0.63 ± 0.09	-0.64 ± 0.15	-0.84 ± 0.03	-0.95 ± 0.12	-1.86 ± 0.82
Ny Ålesund	-0.81 ± 0.23	-0.50 ± 0.10	-0.46 ± 0.15	-0.84 ± 0.03	-1.08 ± 0.12	-1.41 ± 0.96
Thule	-1.21 ± 0.31	-0.61 ± 0.09	-0.53 ± 0.15	-0.84 ± 0.03	-0.94 ± 0.12	-1.61 ± 0.85
Kiruna	-1.05 ± 0.36	-0.41 ± 0.10	-0.42 ± 0.16	-0.83 ± 0.02	-0.96 ± 0.12	-1.62 ± 0.86
Poker Flat	-1.56 ± 0.64	-0.46 ± 0.09	-0.63 ± 0.11	-0.83 ± 0.02	-0.90 ± 0.09	-1.87 ± 0.60
Harestua	-0.44 ± 0.40	-0.43 ± 0.10	-0.59 ± 0.15	-0.83 ± 0.03	-0.90 ± 0.10	-1.65 ± 0.73
Zugspitze	-0.63 ± 0.19	-0.34 ± 0.08	-0.61 ± 0.13	-0.85 ± 0.02	-0.91 ± 0.09	-1.87 ± 0.56
Jungfraujoch	-0.98 ± 0.16	-0.34 ± 0.07	-0.64 ± 0.12	-0.86 ± 0.02	-0.93 ± 0.09	-1.80 ± 0.56
Toronto	-1.22 ± 0.37	-0.22 ± 0.11	-0.34 ± 0.19	-0.80 ± 0.02	-1.08 ± 0.15	-0.03 ± 1.44
Tsukuba	-1.00 ± 0.25	-0.48 ± 0.07	-0.73 ± 0.16	-0.89 ± 0.02	-0.93 ± 0.10	-0.30 ± 0.56
Kitt Peak	-1.03 ± 0.53	-0.42 ± 0.06	-0.62 ± 0.12	-0.90 ± 0.03	-0.95 ± 0.09	-1.75 ± 0.38
Izaña	-0.66 ± 0.15	-0.37 ± 0.06	-0.53 ± 0.12	-0.91 ± 0.04	-0.87 ± 0.08	-1.48 ± 0.39
Mauna Loa	-0.39 ± 0.19	-0.03 ± 0.05	-0.35 ± 0.11	-0.90 ± 0.03	-1.22 ± 0.06	0.18 ± 0.72
Wollongong	-0.55 ± 0.16	-0.95 ± 0.05	-0.74 ± 0.13	-0.87 ± 0.02	-0.96 ± 0.09	-1.26 ± 0.50
Lauder	-0.60 ± 0.21	-0.96 ± 0.07	-0.79 ± 0.12	-0.85 ± 0.02	-0.97 ± 0.09	-1.78 ± 0.67
Arrival Heights	-0.36 ± 0.67	-1.09 ± 0.08	-0.74 ± 0.13	-0.97 ± 0.15	-0.87 ± 0.09	-1.32 ± 1.26

Table 5. $ClONO_2$ trend in % per year between 2000 and 2009, calculated by fitting a linear function combined with a first (sites poleward of 70°) or third order Fourier series to the data. The error bars were determined with the bootstrap method.

Measurement site	FTIR	KASIMA	SLIMCAT	2-D model	EMAC	SOCOL
Eureka	-4.56 ± 0.78	-1.18 ± 0.19	-0.83 ± 0.25	-1.21 ± 0.10	-1.75 ± 0.16	-3.37 ± 2.87
Ny Ålesund	6.79 ± 5.01	-1.03 ± 0.20	-0.62 ± 0.26	-1.20 ± 0.08	-1.59 ± 0.17	-1.84 ± 3.07
Thule	-3.58 ± 1.04	-1.28 ± 0.18	-0.94 ± 0.25	-1.20 ± 0.07	-1.77 ± 0.16	-3.37 ± 2.46
Kiruna	-1.45 ± 0.95	-0.91 ± 0.16	-0.71 ± 0.24	-1.19 ± 0.04	-1.05 ± 0.17	-1.62 ± 2.36
Harestua	-0.07 ± 0.52	-1.05 ± 0.14	-0.80 ± 0.21	-1.21 ± 0.03	-1.01 ± 0.16	-2.73 ± 1.58
Zugspitze	-1.37 ± 0.52	-0.90 ± 0.12	-0.02 ± 0.24	-1.24 ± 0.05	-1.16 ± 0.15	-3.42 ± 0.62
Jungfraujoch	-1.44 ± 0.33	-0.90 ± 0.12	-0.06 ± 0.22	-1.25 ± 0.05	-1.16 ± 0.15	-3.30 ± 0.61
Kitt Peak	-2.53 ± 1.16	-0.86 ± 0.08	-0.21 ± 0.18	-1.31 ± 0.05	-1.14 ± 0.12	-2.89 ± 0.67
Izaña	-2.86 ± 0.67	-0.72 ± 0.10	0.19 ± 0.16	-1.33 ± 0.08	-1.14 ± 0.10	-2.14 ± 0.66
Wollongong	-2.18 ± 0.60	-1.47 ± 0.07	-0.96 ± 0.16	-1.25 ± 0.04	-1.54 ± 0.11	-1.46 ± 0.92
Lauder	-0.35 ± 0.46	-1.61 ± 0.09	-0.59 ± 0.20	-1.22 ± 0.05	-1.18 ± 0.16	-2.21 ± 0.74
Arrival Heights	0.99 ± 0.76	-1.65 ± 0.20	-1.11 ± 0.26	-0.84 ± 0.82	-0.52 ± 0.23	-1.54 ± 3.71

the pole. At the Northern Hemisphere sites, the measurements show a much weaker increase of HF than KASIMA and SLIMCAT, at some sites even a decrease.

7 Discussion

Total column abundances of HCl, $ClONO_2$, and HF were determined from FTIR measurements at 17 sites between 80.05° N and 77.82° S and compared to the calculations of five different models with focus on the time period 2000–2009. Different aspects should be considered and discussed before the trends calculated from the FTIR measurements and model data for this study are interpreted and compared.

The offset in the absolute values between models and measurements seen in Sect. 4 is assumed to be constant in time and sufficiently small so that it does not strongly influence the trend result.

In contrast, the FTIR trends depend on whether or not a Fourier series is incorporated in the fitting function to account for the seasonal cycle, although the different results mostly agree within their errors (Sect. 5.2). Because the seasonal cycle of the investigated gases is very pronounced, especially in polar regions, and the time series considered are not very long, the trends calculated without including the Fourier series depend on the start and end time of year.

When the FTIR data are restricted to a period with less variability, in this case summer and autumn (corresponding to June to November in the Northern and December to May in the Southern Hemisphere), the error bars are quite large so that an agreement with the trends from the complete time series is found at most of the sites (Sect. 5.2). One reason

Table 6. HF trend in % per year between 2000 and 2009, calculated by fitting a linear function combined with a first (sites poleward of 70°) or third order Fourier series to the data. The error bars were determined with the bootstrap method.

Measurement site	FTIR	KASIMA	SLIMCAT	2-D model
Eureka	-0.56 ± 0.69	0.76 ± 0.11	0.79 ± 0.11	0.23 ± 0.03
Ny Ålesund	0.61 ± 0.70	0.85 ± 0.10	0.93 ± 0.11	0.23 ± 0.03
Thule	-1.11 ± 0.54	0.74 ± 0.11	0.83 ± 0.11	0.22 ± 0.03
Kiruna	0.61 ± 0.42	0.94 ± 0.12	0.96 ± 0.15	0.22 ± 0.04
Poker Flat	1.54 ± 1.18	1.22 ± 0.11	1.41 ± 0.15	0.21 ± 0.04
Harestua	-0.02 ± 0.54	0.93 ± 0.12	0.93 ± 0.16	0.19 ± 0.03
Zugspitze	0.95 ± 0.32	1.10 ± 0.10	1.24 ± 0.16	0.14 ± 0.05
Jungfraujoch	0.48 ± 0.25	1.11 ± 0.10	1.22 ± 0.15	0.14 ± 0.05
Toronto	-0.04 ± 0.61	1.04 ± 0.14	1.45 ± 0.25	0.00 ± 0.05
Tsukuba	0.31 ± 0.34	0.96 ± 0.08	1.00 ± 0.19	0.09 ± 0.04
Kitt Peak	0.55 ± 0.68	1.20 ± 0.07	1.27 ± 0.15	0.08 ± 0.04
Izaña	0.92 ± 0.21	1.43 ± 0.07	1.66 ± 0.15	0.06 ± 0.06
Mauna Loa	0.43 ± 0.30	2.32 ± 0.09	2.11 ± 0.15	0.03 ± 0.05
Wollongong	1.61 ± 0.31	0.80 ± 0.07	1.15 ± 0.15	0.14 ± 0.04
Lauder	1.07 ± 0.28	0.81 ± 0.08	1.27 ± 0.15	0.19 ± 0.04
Arrival Heights	0.68 ± 0.58	1.14 ± 0.10	1.38 ± 0.09	0.26 ± 0.04

for the large error bars is probably that there is still some variability left in the summer data. Furthermore, some of the time series contain only few data points during this time of year probably due to the weather conditions and because at some sites, the measurements have been performed on a campaign basis.

All FTIR sites taking part in this study except La Réunion and Toronto started operation before the year 2000. This is why for the more thorough investigation, the time period 2000 to 2009 was chosen so that nearly all measurement time series have the same length. Of course, the error bars for the longer period between 1996 and 2009 are usually smaller when compared for the sites where operation was started before or in 1996 (Sect. 5.3). The trends calculated for the six-year period 2004 to 2009 are probably not significant in terms of Weatherhead et al. (1998). As discussed by Weatherhead et al. (1998), the length of a time series necessary to determine a certain trend depends on the magnitude of the expected trend, the standard deviation, and the autocorrelation of the time series. The trends expected here are quite small and the standard deviations quite large, especially in polar regions, where the Fourier series does not fully capture the amplitude of the seasonal cycle, especially for $ClONO_2$. The autocorrelation is not easy to determine because the time series are not continuous.

Still, when comparing the trends from models and measurements, it must be considered that the time ranges do not always agree exactly, especially for Poker Flat whose measurement series ends in 2004, and for Toronto where the trends from 2002–2009 are compared with those for 2000–2009 from the other sites. Concerning the models, the time series from SOCOL ends in 2004, and the one from the 2-D model in 2008 for all species at all sites. Moreover, in contrast to the model output, the sampling of the FTIR data is not regular because the instrument needs clear sky conditions and the sun above the horizon so that it cannot measure in cloudy weather and during polar night.

The trends determined for HCl and $ClONO_2$ (roughly around -1 to $-2\,\%\,yr^{-1}$) agree very well with those presented by the WMO (2011) for the stratospheric inorganic halogen abundance (EESC = Equivalent Effective Stratospheric Chlorine) estimated from tropospheric measurements of ozone-depleting substances. This EESC was calculated from the chlorine- and bromine-containing source gases by accounting for the transport time to the stratosphere and considering the dependency of the fractional release values on the mean age-of-air (Newman et al., 2007). A decrease of midlatitude EESC of 11 % between the peak in 1997 and 2008 is reported by the WMO (2011) corresponding to a trend of about $-1\,\%\,yr^{-1}$. The peak in the Antarctic polar vortex occurred later, in 2002. Until 2008, the EESC abundance decreased by about 5 % there (WMO, 2011) which corresponds to a trend of about $-0.8\,\%\,yr^{-1}$. This slightly weaker decrease in the southern high latitudes cannot be seen clearly in the FTIR measurements analysed and presented here. Two models (EMAC and the 2-D model) show this tendency towards weaker $ClONO_2$ and EMAC also towards weaker HCl trends when approaching the south pole for the 2000–2009 trends (Sect. 6).

The present study is also able to confirm the results of many other preceding investigations on stratospheric inorganic chlorine and fluorine measurements. The stabilisation of the stratospheric HCl content at the end of the 1990s described in Sect. 4.1 was already seen for example by Considine et al. (1999), Rinsland et al. (2003), and Newchurch et al. (2003). Also the subsequent negative trend in the

stratospheric chlorine abundance was reported before by other studies. For example, Lary et al. (2007) found a decrease towards the end of their study in which they analysed a stratospheric Cl_y time series between 1991 and 2006 that was created from a combination of many different (mainly satellite) measurements. For HCl, a trend was estimated from measurements made by the MLS (Microwave Limb Sounder) instrument aboard the Aura satellite between 50 and 65 km height and 60° S and 60° N by Froidevaux et al. (2006). They reported a decrease in the volume mixing ratio of (-0.78±0.08)% yr^{-1} between August 2004 and January 2006. This value also agrees very well with those found in the present study. A similar result for HCl was published by Jones et al. (2011) who combined HALOE (Halogen Occultation Experiment) data with ACE-FTS (Atmospheric Chemistry Experiment Fourier Transform Spectrometer) results between 35 and 45 km to form a time series of HCl from 1993 to 2008. They found a significantly negative trend of about -5.1 % $decade^{-1}$ to -5.8 % $decade^{-1}$ for the time period 1997–2008, depending on latitude. Measurements with the McMath-Pierce solar telescope on Kitt Peak (Arizona, US) showed a slightly larger decrease of the HCl total column abundance of (-1.8 ± 0.4)% yr^{-1} between 1997 and 2007 (Wallace and Livingston, 2007). Concerning the HF total column abundance, a strong increase of (10.9 ± 1.1)% yr^{-1} above Kitt Peak between 1977 and 1990 was reported by Rinsland et al. (1991). It weakened during the 1990s so that the trend for the period 1977–2001 amounted to (4.30 ± 0.15)% yr^{-1} only (Rinsland et al., 2002). A leveling-off could be seen by Zander et al. (2008) above Jungfraujoch around 2003–2004. This agrees very well with the results of the present study at some of the northern hemisphere sites, where the HF trends are much weaker for the period 2004–2009 than for 2000–2009 and 1996–2009, or even negative (Sect. 5.3).

Part of the discrepancy between the modelled trends can be explained by the different halocarbon scenarios used in the simulations. Considering a time shift of a few years due to the transport of CCl_y and CF_y from the surface to the stratosphere, the weakest chlorine decrease in 2000–2009 would be expected from the WMO (2007) Ref 2 scenario used by KASIMA and the 2-D model (Fig. 1). KASIMA indeed at most sites shows the weakest decrease in HCl and $ClONO_2$, along with SLIMCAT (Fig. 12 and Tables 4 and 5). In contrast, the 2-D model shows a stronger decrease than expected from the scenario. Above most of the measurement sites, also EMAC and SOCOL show stronger HCl and $ClONO_2$ decreases than expected from the surface halocarbon scenarios they used. For HF, the 2-D model calculated much weaker increases than KASIMA and SLIMCAT did (Fig. 12 and Tab. 6). This cannot be explained by the different scenarios because as already mentioned, KASIMA and the 2-D model used the same one. A possible reason for a part of this discrepancy in the HF trends is the fact that the 2-D model does not treat all halogen-containing species explicitly (please see Sect. 3.1). Instead, the mixing ratios of some are added proportionately to those of others with similar lifetimes by considering the number of chlorine atoms. But this means that for some gases, the contained amount of fluorine is not represented correctly so that very roughly about 50 pptv are missing in the surface CF_y mixing ratio. As the missing amount of CF_y increases with time, the trend of the HF total column abundance is expected to be slightly too small in the 2-D model.

The trends of HCl, $ClONO_2$, and HF between 2000 and 2009 have been examined with respect to differences between the hemispheres (Sect. 6). The FTIR measurements suggest a stronger decrease of HCl and $ClONO_2$ in the Northern Hemisphere than in the Southern Hemisphere, while the models, except KASIMA, do not show a hemispheric dependency. However, the KASIMA signal is inverse to the FTIR one: the relative decrease is stronger in the Southern Hemisphere. According to the measurements, the HF total column abundances in the Southern Hemisphere still increase while the sites in the Northern Hemisphere show a more differentiated picture. There are some with positive trends as well, especially in the low latitudes, but also some without a significant trend. In the high latitudes, there are two sites showing a negative trend. This tendency towards a HF stabilisation or even decrease in the Northern Hemisphere in the last few years is also visible in other FTIR time series for the later and shorter period 2004–2009 (Sect. 5.3). In contrast, the models show a more or less strong increase of HF at all locations without a discernible difference between the hemispheres.

At some sites, the trends of HCl and $ClONO_2$ show significant discrepancies in magnitude (Sect. 6). This was already described by Kohlhepp et al. (2011) for Kiruna and in the SPARC CCMVal (2010) report for the Jungfraujoch. In Kiruna, the trends between 1996 and 2009 of these two gases differ by about a factor of four both for the FTIR measurements and the KASIMA model calculations (Kohlhepp et al., 2011). When extending this investigation for Kiruna by the other 16 sites and four models in the present study, a latitudinal dependency of the difference can be found in the FTIR measurements in the Northern Hemisphere. In the low and high latitudes, $ClONO_2$ decreases much faster than HCl, while in the midlatitudes, it decreases only slightly faster. Concerning the difference between high and midlatitudes, EMAC and SOCOL and to a certain degree also SLIMCAT show a similar signal, while the other models do not show a distinct latitudinal dependency but a slightly stronger decrease of $ClONO_2$ at all sites.

8 Conclusions

There is an overall agreement between the models and measurements in a decrease of HCl and $ClONO_2$ during the period 2000–2009, as is expected from the ban or restrictions

on the production of the anthropogenic chlorine source gases (e.g. CFCs and HCFCs) in the Montreal Protocol and its amendments and adjustments. Because fluorine emission is not explicitly restricted, the HF total column abundances are expected to be still increasing, which can be seen especially in the model simulations. The measurements also confirm this, but suggest a stabilisation of HF in the last few years, at least in the Northern Hemisphere.

The models tend to underestimate the decrease seen in the HCl and $ClONO_2$ measurements in the Northern Hemisphere and to overestimate it in the Southern Hemisphere. Analogously, they tend to overestimate the increase of HF in the Northern Hemisphere. The FTIR trend results depend both on hemisphere and on latitude, while the models do not show distinct differences between the hemispheres, but most of them simulate a dependency on latitude.

Supplementary material related to this article is available online at: http://www.atmos-chem-phys.net/12/3527/2012/acp-12-3527-2012-supplement.pdf.

Acknowledgements. We thank the NASA Goddard Space Flight Center for providing NCEP daily temperature and pressure profiles (via the automailer system) which were used for the calibration and inversion of the FTIR spectra at most of the measurement sites.

The PEARL Bruker 125HR measurements at Eureka were made by the Canadian Network for the Detection of Atmospheric Change (CANDAC) and in part by the Canadian Arctic ACE Validation Campaigns, and were supported by the Atlantic Innovation Fund/Nova Scotia Research Innovation Trust, Canada Foundation for Innovation, Canadian Foundation for Climate and Atmospheric Sciences, Canadian Space Agency, Environment Canada, Government of Canada International Polar Year funding, Natural Sciences and Engineering Research Council, Northern Scientific Training Program, Ontario Innovation Trust, Polar Continental Shelf Program, and Ontario Research Fund. For the DA8 measurements at Eureka we gratefully acknowledge the collaborative effort between the Japan Meteorological Agency (JMA) and Environment Canada, and the financial support provided by the Canadian Foundation for Climate and Atmospheric Science to the University of Toronto for our joint measurement program at Eureka in 2002–2003. The recording of DA8 atmospheric solar absorption spectra, from 2004 to 2008, was made possible through collaboration with the Atmospheric Chemistry Experiment (ACE) Arctic Validation Team. The authors wish to thank the staff at the Eureka weather station and CANDAC for the logistical and on-site support provided at Eureka.

The National Center for Atmospheric Research is supported by the National Science Foundation. The NCAR FTS observation program at Thule, GR is supported under contract by the National Aeronautics and Space Administration (NASA). This work is also supported by the NSF Office of Polar Programs (OPP). The Mauna Loa FTS program is supported by the National Aeronautics and Space Administration. We wish to thank the Danish Meteorological Institute for support at the Thule site.

The TAO Bomem DA8 measurements were supported by ABB Bomem, the Canada Foundation for Innovation, Canadian Foundation for Climate and Atmospheric Science, Canadian Space Agency, Environment Canada, Natural Science and Engineering Research Council, Ontario Research and Development Challenge Fund, Premier's Research Excellent Award, and University of Toronto.

The University of Liège contribution to the present work has primarily been supported by the SECPEA and A3C PRODEX projects funded by the Belgian Federal Science Policy Office (BELSPO, Brussels). The ULg team further acknowledges the International Foundation High Altitude Research Stations Jungfraujoch and Gornergrat (HFSJG, Bern) for supporting the facilities needed to perform the observations. E. Mahieu is Research Associate with the F.R.S.-FNRS (Fonds de la Recherche Scientifique, Brussels, Belgium).

We acknowledge the support of the European Commission through GEOmon (contract number FP6-2005-Global-4-036677) and HYMN (contract no. 037048 (GOCE)) projects under the 6th Framework Programme.

We further acknowledge support by Deutsche Forschungsgemeinschaft and Open Access Publishing Fund of Karlsruhe Institute of Technology.

Finally, we wish to thank the Editor J. B. Burkholder and two anonymous reviewers very much for their helpful and constructive comments regarding our manuscript.

Edited by: J. B. Burkholder

References

Atkinson, R., Baulch, D. L., Cox, R. A., Crowley, J. N., Hampson, R. F., Hynes, R. G., Jenkin, M. E., Rossi, M. J., and Troe, J.: Evaluated kinetic and photochemical data for atmospheric chemistry: Volume I – gas phase reactions of O_x, HO_x, NO_x and SO_x species, Atmos. Chem. Phys., 4, 1461–1738, doi:10.5194/acp-4-1461-2004, 2004.

Atkinson, R., Baulch, D. L., Cox, R. A., Crowley, J. N., Hampson, R. F., Hynes, R. G., Jenkin, M. E., Rossi, M. J., Troe, J., and IUPAC Subcommittee: Evaluated kinetic and photochemical data for atmospheric chemistry: Volume II – gas phase reactions of organic species, Atmos. Chem. Phys., 6, 3625–4055, doi:10.5194/acp-6-3625-2006, 2006.

Batchelor, R. L., Strong, K., Lindenmaier, R., Mittermeier, R. L., Fast, H., Drummond, J. R., and Fogal, P. F.: A new Bruker IFS 125HR FTIR spectrometer for the Polar Environment Atmospheric Research Laboratory at Eureka, Canada – measurements and comparison with the existing Bomem DA8 spectrometer, J. Atmos. Ocean. Tech., 26, 1328–1340, doi:10.1175/2009JTECHA1215.1, 2009.

Batchelor, R. L., Kolonjari, F., Lindenmaier, R., Mittermeier, R. L., Daffer, W., Fast, H., Manney, G., Strong, K., and Walker, K. A.: Four Fourier transform spectrometers and the Arctic polar vortex: instrument intercomparison and ACE-FTS validation at Eureka during the IPY springs of 2007 and 2008, Atmos. Meas. Tech., 3, 51–66, doi:10.5194/amt-3-51-2010, 2010.

Bian, H. and Prather, M. J.: Fast-J2: Accurate simulation of stratospheric photolysis in global chemical models, J. Atmos. Chem., 41, 281–296, 2002.

Blumenstock, T., Kopp, G., Hase, F., Hochschild, G., Mikuteit, S., Raffalski, U., and Ruhnke, R.: Observation of unusual chlorine activation by ground-based infrared and microwave spectroscopy in the late Arctic winter 2000/01, Atmos. Chem. Phys., 6, 897–905, doi:10.5194/acp-6-897-2006, 2006.

Brault, J. W.: Solar Fourier transform spectroscopy, in Proceedings of the JOSO Workshop, Future Solar Optical Observations, Needs and Constraints, edited by: Godoli, G., Noci, G., and Righin, A., 33–52, Florence, Italy, 1978.

Brown, L. R., Gunson, M. R., Toth, R. A., Irion, F. W., Rinsland, C. P., and Goldman, A.: Atmospheric Trace Molecule Spectroscopy (ATMOS) linelist, Appl. Optics, 35, 2828–2848, 1996.

Chipperfield, M. P., Burton, M., Bell, W., Paton Walsh, C., Blumenstock, Th., Coffey, M. T., Hannigan, J. W., Mankin, W. G., Galle, B., Mellqvist, J., Mahieu, E., Zander, R., Notholt, J., Sen, B., and Toon, G. C.: On the use of HF as a reference for the comparison of stratospheric observations and models, J. Geophys. Res., 102, 12901–12919, 1997.

Chipperfield, M. P.: Multiannual simulations with a three-dimensional chemical transport model, J. Geophys. Res., 104, 1781–1805, 1999.

Chipperfield, M. P. and Feng, W.: Comment on: Stratospheric Ozone Depletion at northern mid-latitudes in the 21st century: The importance of future concentrations of greenhouse gases nitrous oxide and methane, Geophys. Res. Lett., 30, 1389, doi:10.1029/2002GL016353, 2003.

Chipperfield, M. P.: New Version of the TOMCAT/SLIMCAT Off-Line Chemical Transport Model: Intercomparison of Stratospheric Tracer Experiments, Q. J. Roy. Meteorol. Soc., 132, 1179–1203, doi:10.1256/qj.05.51, 2006.

Coffey, M. T., Goldman, A., Hannigan, J. W., Mankin, W. G., Schoenfeld, W. G., Rinsland, C. P., Bernardo, C., and Griffith, D. W. T. : NOTE: Improved Vibration-Rotation (0-1) HBr Line Parameters for Validating High Resolution Infrared Atmospheric Spectra Measurements, J. Quant. Spectrosc. Ra., 60, 863–867, 1998

Considine, G. D., Deaver, L. E., Remsberg, E. E., and Russell, J. M. III: Analysis of near-global trends and variability in Halogen Occultation Experiment HF and HCl data in the middle atmosphere, J. Geophys. Res., 104, 24297–24308, 1999.

Crutzen, P. J., Isaksen, I. S. A., and McAfee, J. R.: The impact of the chlorocarbon industry on the ozone layer, J. Geophys. Res., 83, 345–363, 1978.

Duchatelet, P., Demoulin, P., Hase, F., Ruhnke, R., Feng, W., Chipperfield, M. P., Bernath, P. F., Boone, C. D., Walker, K. A., and Mahieu, E.: Hydrogen fluoride total and partial column time series above the Jungfraujoch from long-term FTIR measurements: Impact of the line-shape model, characterization of the error budget and seasonal cycle, and comparison with satellite and model data, J. Geophys. Res., 115, D22306, doi:10.1029/2010JD014677, 2010.

Egorova, T. A., Rozanov, E. V., Zubov, V. A., and Karol, I. L.: Model for investigating ozone trends (MEZON), Atmos. Ocean. Phys., 39, 277–292, 2003.

Egorova, T., Rozanov, E., Zubov, V., Manzini, E., Schmutz, W., and Peter, T.: Chemistry-climate model SOCOL: a validation of the present-day climatology, Atmos. Chem. Phys., 5, 1557–1576, doi:10.5194/acp-5-1557-2005, 2005.

Eyring, V., Butchart, N., Waugh, D. W., Akiyoshi, H., Austin, J., Bekki, S., Bodeker, G. E., Boville, B. A., Brühl, C., Chipperfield, M. P., Cordero, E., Dameris, M., Deushi, M., Fioletov, V. E., Frith, S. M., Garcia, R. R., Gettelman, A., Giorgetta, M. A., Grewe, V., Jourdain, L., Kinnison, D. E., Mancini, E., Manzini, E., Marchand, M., Marsh, D. R., Nagashima, T., Newman, P. A., Nielsen, J. E., Pawson, S., Pitari, G., Plummer, D. A., Rozanov, E., Schraner, M., Shepherd, T. G., Shibata, K., Stolarski, R. S., Struthers, H., Tian, W., and Yoshiki, M.: Assessment of temperature, trace species, and ozone in chemistry-climate model simulations of the recent past, J. Geophys. Res., 111, D22308, doi:22310.21029/22006JD007327, 2006.

Eyring, V., Waugh, D. W., Bodeker, G. E., Cordero, E., Akiyoshi, H., Austin, J., Beagley, S. R., Boville, B. A., Braesicke, P., Brühl, C., Butchart, N., Chipperfield, M. P., Dameris, M., Deckert, R., Deushi, M., Frith, S. M., Garcia, R. R., Gettelman, A., Giorgetta, M. A., Kinnison, D. E., Mancini, E., Manzini, E., Marsh, D. R., Matthes, S., Nagashima, T., Newman, P. A., Nielsen, J. E., Pawson, S., Pitari, G., Plummer, D. A., Rozanov, E., Schraner, M., Scinocca, J. F., Semeniuk, K., Shepherd, T. G., Shibata, K., Steil, B., Stolarski, R. S., Tian, W., and Yoshiki, M.: Multi-model projections of stratospheric ozone in the 21st century, J. Geophys. Res., 112, D16303, doi:16310.11029/12006JD008332, 2007.

Eyring, V., Chipperfield, M. P., Giorgetta, M. A., Kinnison, D. E., Manzini, E., Matthes, K., Newman, P. A., Pawson, S., Shepherd, T. G., and Waugh, D. W.: Overview of the New CCMVal Reference and Sensitivity Simulations in Support of Upcoming Ozone and Climate Assessments and the Planned SPARC CCMVal Report, SPARC Newsletter, 30, 20–26, 2008.

Fast, H., Mittermeier, R. L., and Makino, Y.: A ten-year record of Arctic trace gas total column measurements at Eureka, Canada, from 1997 to 2006, Atmos.-Ocean, 49, 67–94, doi:10.1080/07055900.2011.562470, 2011.

Feng, W., Chipperfield, M. P., Dorf, M., Pfeilsticker, K., and Ricaud, P.: Mid-latitude ozone changes: studies with a 3-D CTM forced by ERA-40 analyses, Atmos. Chem. Phys., 7, 2357–2369, doi:10.5194/acp-7-2357-2007, 2007.

Froidevaux, L., Livesey, N. J., Read, W. G., Salawitch, R. J., Waters, J. W., Drouin, B., MacKenzie, I. A., Pumphrey, H. C., Bernath, P., Boone, C., Nassar, R., Montzka, S., Elkins, J., Cunnold, D., and Waugh, D.: Temporal decrease in upper atmospheric chlorine, Geophys. Res. Lett., 33, L23812, doi:10.1029/2006GL027600, 2006.

Gardiner, T., Forbes, A., de Mazière, M., Vigouroux, C., Mahieu, E., Demoulin, P., Velazco, V., Notholt, J., Blumenstock, T., Hase, F., Kramer, I., Sussmann, R., Stremme, W., Mellqvist, J., Strandberg, A., Ellingsen, K., and Gauss, M.: Trend analysis of greenhouse gases over Europe measured by a network of ground-based remote FTIR instruments, Atmos. Chem. Phys., 8, 6719–6727, doi:10.5194/acp-8-6719-2008, 2008.

Goldman, A., Paton-Walsh, C., Bell, W., Toon, G. C., Blavier, J.-F., Sen, B., Coffey, M. T., Hannigan, J. W., and Mankin, W. G.: Network for the detection of stratospheric change Fourier transform infrared intercomparison at Table Mountain Facility, November 1996, J. Geophys. Res., 104, 30481–30503, 1999.

Griffith, D. W. T., Jones, N. B., and Matthews, W. A.: Interhemispheric ratio and Annual Cycle of Carbonyl Sulphide (OCS) Total Column from Ground-Based FTIR Spectra, J. Geophys. Res., 103, 8447–8454, 1998.

Hannigan, J. W., Coffey, M. T., and Goldman, A.: Semi-Autonomous FTS Observation System for Stratospheric and Tropospheric Gases, J. Atmos. Oceanic Technol., 26, 1814–1828, 2009.

Hase, F., Blumenstock, T., and Paton-Walsh, C.: Analysis of the instrumental lineshape of high-resolution Fourier transform IR spectrometers with gas cell measurements and new retrieval software, Appl. Optics, 38, 3417–3422, 1999.

Hase, F., Hannigan, J. W., Coffey, M. T., Goldman, A., Höpfner, M., Jones, N. B., Rinsland, C. P., and Wood, C. P.: Intercomparison of retrieval codes used for the analysis of high-resolution, ground-based FTIR measurements, J. Quant. Spectrosc. Ra., 87, 25–52, 2004.

Hossaini, R., Chipperfield, M. P., Monge-Sanz, B. M., Richards, N. A. D., Atlas, E., and Blake, D. R.: Bromoform and dibromomethane in the tropics: a 3-D model study of chemistry and transport, Atmos. Chem. Phys., 10, 719–735, doi:10.5194/acp-10-719-2010, 2010.

IPCC (Intergovernmental Panel on Climate Change): Climate Change 2001: Synthesis Report. A Contribution of Working Groups I, II and III to the Third Assessment Report of the Intergovernmental Panel on Climate Change, edited by: Watson, R. T. and the Core Writing Team, Cambridge University Press, Cambridge, UK, and New York, USA, 2001.

IPCC (Intergovernmental Panel on Climate Change): Climate Change 2007: Synthesis Report. A Contribution of Working Groups I, II and III to the Fourth Assessment Report of the Intergovernmental Panel on Climate Change, edited by: Core Writing Team, Pachauri, R. K., and Reisinger, A., IPCC, Geneva, Switzerland, 2007.

Jones, A., Urban, J., Murtagh, D. P., Sanchez, C., Walker, K. A., Livesey, N. J., Froidevaux, L., and Santee, M. L.: Analysis of HCl and ClO time series in the upper stratosphere using satellite data sets, Atmos. Chem. Phys., 11, 5321–5333, 2011, http://www.atmos-chem-phys.net/11/5321/2011/.

Jöckel, P., Sander, R., Kerkweg, A., Tost, H., and Lelieveld, J.: Technical Note: The Modular Earth Submodel System (MESSy) – a new approach towards Earth System Modeling, Atmos. Chem. Phys., 5, 433–444, doi:10.5194/acp-5-433-2005, 2005.

Jöckel, P., Tost, H., Pozzer, A., Brühl, C., Buchholz, J., Ganzeveld, L., Hoor, P., Kerkweg, A., Lawrence, M. G., Sander, R., Steil, B., Stiller, G., Tanarhte, M., Taraborrelli, D., van Aardenne, J., and Lelieveld, J.: The atmospheric chemistry general circulation model ECHAM5/MESSy1: consistent simulation of ozone from the surface to the mesosphere, Atmos. Chem. Phys., 6, 5067–5104, doi:10.5194/acp-6-5067-2006, 2006.

Kagawa, A., Kasai, Y., Jones, N. B., Yamamori, M., Seki, K., Murcray, F., Murayama, Y., Mizutani, K., and Itabe, T.: Characteristics and error estimation of stratospheric ozone and ozone-related species over Poker Flat (65° N, 147° W), Alaska observed by a ground-based FTIR spectrometer from 2001 to 2003, Atmos. Chem. Phys., 7, 3791–3810, doi:10.5194/acp-7-3791-2007, 2007.

Kinnersley, J. S.: The climatology of the stratospheric THIN AIR model, Q. J. Roy. Meteorol. Soc., 122, 219–252, 1996.

Kohlhepp, R., Barthlott, S., Blumenstock, T., Hase, F., Kaiser, I., Raffalski, U., and Ruhnke, R.: Trends of HCl, $ClONO_2$, and HF column abundances from ground-based FTIR measurements in Kiruna (Sweden) in comparison with KASIMA model calculations, Atmos. Chem. Phys., 11, 4669–4677, doi:10.5194/acp-11-4669-2011, 2011.

Kouker, W., Langbein, I., Reddmann, T., and Ruhnke, R.: The Karlsruhe Simulation Model of the Middle Atmosphere (KASIMA), Forschungszentrum Karlsruhe, Germany, Version 2, FZK Report 6278, 1999.

Lait, L., Newman, P., and Schoeberl, R.: Using the Goddard Automailer, available at: http://code916.gsfc.nasa.gov/Dataservices, 2005.

Lary, D. J., Waugh, D. W., Douglass, A. R., Stolarski, R. S., Newman, P. A., and Mussa, H.: Variations in stratospheric inorganic chlorine between 1991 and 2006, Geophys. Res. Lett., 34, L21811, doi:10.1029/2007GL030053, 2007.

Mahieu, E., Duchatelet, P., Demoulin, P., Walker, K. A., Dupuy, E., Froidevaux, L., Randall, C., Catoire, V., Strong, K., Boone, C. D., Bernath, P. F., Blavier, J.-F., Blumenstock, T., Coffey, M., De Mazière, M., Griffith, D., Hannigan, J., Hase, F., Jones, N., Jucks, K. W., Kagawa, A., Kasai, Y., Mebarki, Y., Mikuteit, S., Nassar, R., Notholt, J., Rinsland, C. P., Robert, C., Schrems, O., Senten, C., Smale, D., Taylor, J., Tétard, C., Toon, G. C., Warneke, T., Wood, S. W., Zander, R., and Servais, C.: Validation of ACE-FTS v2.2 measurements of HCl, HF, CCl3F and CCl2F2 using space-, balloon- and ground-based instrument observations, Atmos. Chem. Phys., 8, 6199–6221, doi:10.5194/acp-8-6199-2008, 2008.

Manzini, E., McFarlane, N. A., and McLandress, C.: Impact of the Doppler spread parameterization on the simulation of the middle atmosphere circulation using the MA/ECHAM4 general circulation model, J. Geophys. Res., 102, 25751–25762, 1997.

McPeters, R. D., Hofmann, D. J., Clark, M., Flynn, L., Froidevaux, L., Gross, M., Johnson, B., Koenig, G., Liu, X., McDermid, S., McGee, T., Murcray, F., Newchurch, M. J., Oltmans, A., Parrish, A., Schnell, R., Singh, U., Tsou, J. J., Walsh, T., and Zawodny, J. M.: Results from the 1995 Stratospheric Ozone Profile Intercomparison at Mauna Loa, J. Geophys. Res., 104, 30505–30514, 1999.

Meier, A., Paton-Walsh, C., Bell, W., Blumenstock, T., Hase, F., Goldman, A., Steen, A., Kift, R., Woods, P., and Kondo, Y.: Evidence of reduced measurement uncertainties from an FTIR instrument intercomparison at Kiruna, Sweden, J. Quant. Spectrosc. Ra., 96, 75–84, 2005.

Mikuteit, S.: Trendbestimmung stratosphärischer Spurengase mit Hilfe bodengebundener FTIR-Messungen, Wissenschaftliche Berichte, FZKA-Report No. 7385, Forschungszentrum Karlsruhe, Germany, 2008.

Molina, M. J. and Rowland, F. S.: Stratospheric sink for chlorofluoromethanes: chlorine atom-catalysed destruction of ozone, Nature 249, 810–812, 1974.

Monge-Sanz, B., Chipperfield, M. P., Simmons, A., and Uppala, S.: Mean age of air and transport in a CTM: Comparison of different ECMWF analyses, Geophys. Res. Lett., 34, L04801, doi:10.1029/2006GL028515, 2007.

Morgenstern, O., Giorgetta, M. A., Shibata, K., Eyring, V., Waugh, D. W., Shepherd, T. G., Akiyoshi, H., Austin, J., Baumgaertner, A. J. G., Bekki, S., Braesicke, P., Brühl, C., Chipperfield, M. P., Cugnet, D., Dameris, M., Dhomse, S., Frith, S. M., Garny, H., Gettelman, A., Hardiman, S. C., Hegglin, M. I., Jöckel, P., Kinnison, D. E., Lamarque, J.-F., Mancini, E., Manzini, E., Marchand, M., Michou, M., Nakamura, T., Nielsen, J. E., Olivié, D.,

Pitari, G., Plummer, D. A., Rozanov, E., Scinocca, J. F., Smale, D., Teyssèdre, H., Toohey, M., Tian, W., and Yamashita, Y.: Review of present-generation stratospheric chemistry-climate models and associated external forcings, J. Geophys. Res., 115, D00M02, doi:10.1029/2009JD013728, 2010.

Murata, I., Nakajima, H., Nakane, H., and Fukunishi, H.: Temporal variations of HCl, HF, O_3, and HNO_3 observed at Tsukuba with Fourier transform spectrometer, Proceedings of the 6th International Conference on Global Change: Connection to the Arctic, 59–62, 2005.

Nakicenovic, N., Alcamo, J., Davis, G., de Vries, B., Fenhann, J., Gaffin, S., Gregory, K., Grübler, A., Jung, T.Y., Kram, T., Lebre La Rovere, E., Michaelis, L., Mori, S., Morita, T., Pepper, W., Pitcher, H., Price, L., Riahi, K., Roehrl, A., Rogner, H.-H., Sankovski, A., Schlesinger, M., Shukla, P., Smith, S., Swart, R., van Rooijen, S., Victor, N., and Dadi, Z.: Special Report on Emissions Scenarios: A Special Report of Working Group III of the Intergovernmental Panel on Climate Change, Cambridge University Press, Cambridge, UK, 599 pp., available at: http://www.grida.no/climate/ipcc/emission/index.htm, 2000.

Newchurch, M. J., Yang, E.-S., Cunnold, D. M., Reinsel, G. C., Zawodny, J. M., and Russell, J. M. III: Evidence for slowdown in stratospheric ozone loss: First stage of ozone recovery, J. Geophys. Res., 108, 4507, doi:10.1029/2003JD003471, 2003.

Newman, P. A., Daniel, J. S., Waugh, D. W., and Nash, E. R.: A new formulation of equivalent effective stratospheric chlorine (EESC), Atmos. Chem. Phys., 7, 4537–4552, doi:10.5194/acp-7-4537-2007, 2007.

Notholt, J., Meier, A., and Peil, S.: Total Column Densities of Tropospheric and Stratospheric Trace Gases in the Undisturbed Arctic Summer Atmosphere, J. Atmos. Chem., 20, 311–332, 1995.

Notholt, J., von der Gathen, P., and Peil, S.: Heterogeneous conversion of HCl and $ClONO_2$ during the Arctic winter 1992/1993 initiating ozone depletion, J. Geophys. Res., 100, 11269–11274, 1995.

Paton-Walsh, C., Jones, N., Wilson, S., Meier, A., Deutscher, N., Griffith, D., Mitchell, R., and Campbell, S.: Trace gas emissions from biomass burning inferred from aerosol optical depth, Geophys. Res. Lett., 31, L05116, doi:10.1029/2003GL018973, 2004.

Paton-Walsh, C., Jones, N. B., Wilson, S. R., Haverd, V., Meier, A., Griffith, D. W. T., and Rinsland, C. P.: Measurements of trace gas emissions from Australian forest fires and correlations with coincident measurements of aerosol optical depth, J. Geophys. Res.-Atmos., 110, D24305, doi:10.1029/2005JD006202, 2005.

Reddmann, T., Ruhnke, R., and Kouker, W.: Three-dimensional model simulations of SF_6 with mesospheric chemistry, J. Geophys. Res., 106, 14525–14537, 2001.

Reisinger, A. R., Jones, N. B., Matthews, W. A., and Rinsland, C. P.: Southern hemisphere ground based measurements of carbonyl fluoride (COF_2) and hydrogen fluoride (HF): Partitioning between fluoride reservoir species, Geophys. Res. Lett., 21, 797–800, 1994.

Reisinger, A. R., Jones, N. B., Matthews, W. A., and Rinsland, C. P.: Southern hemisphere mid-latitude ground based measurements of $ClONO_2$, method of analysis, seasonal cycle, and long term trend, J. Geophys. Res., 100, 23183–23193, 1995.

Rinsland, C. P., Levine, J. S., Goldman, A., Sze, N. D., Ko, M. K. W., and Johnson, D.W .: Infrared measurements of HF and HCl total column abundances above Kitt Peak, 1977–1990: Seasonal cycles, long-term increases, and comparisons with model calculations, J. Geophys. Res., 96, 15523–15540, 1991.

Rinsland, C. P., Nicholas, B. J., Connor, B. J., Logan, J. A., Pougatchev, N. S., Goldman, A., Murcray, F. J., Stephen, T. M., Pine, A. S., Zander, R., Mahieu, E., and Demoulin, P.: Northern and southern hemisphere ground-based infrared spectroscopic measurements of tropospheric carbon monoxide and ethane, J. Geophys. Res., 103, 28197–28218, doi:10.1029/98JD02515, 1998.

Rinsland, C. P., Zander, R., Mahieu, E., Chiou, L. S., Goldman, A., and Jones, N. B.: Stratospheric HF column abundances above Kitt Peak (31.9° N latitude): trends from 1977 to 2001 and correlations with stratospheric HCl columns, J. Quant. Spectrosc. Ra., 74, 205–216, 2002.

Rinsland, C. P., Mahieu, E., Zander, R., Jones, N. B., Chipperfield, M. P., Goldman, A., Anderson, J., Russell III, J. M., Demoulin, P., Notholt, J., Toon, G. C., Blavier, J.-F., Sen, B., Sussmann, R., Wood, S. W., Meier, A., Griffith, D. W. T., Chiou, L. S., Murcray, F. J., Stephen, T. M., Hase, F., Mikuteit, S., Schulz, A., and Blumenstock, T.: Long-term trends of inorganic chlorine from ground-based infrared solar spectra: Past increases and evidence for stabilisation, J. Geophys. Res., 108, 4252, doi:10.1029/2002JD003001, 2003.

Rodgers, C. D.: Inverse Methods for Atmospheric Sounding: Theory and Practice, Series on Atmospheric, Oceanic and Planetary Physics, Vol. 2, World Scientific, Singapore, 2000.

Roeckner, E., Brokopf, R., Esch, M., Giorgetta, M., Hagemann, S., Koernblueh, L., Manzini, E., Schlese, U., and Schulzweida, U.: Sensitivity of simulated climate to horizontal and vertical resolution in the ECHAM5 atmosphere model, J. Climate, 19, 3771–3791, 2006.

Rothman, L. S., Gamache, R. R., Tipping, R. H., Rinsland, C. P., Smith, M. A. H., Chris Benner, D., Malathy Devi, V., Flaud, J.-M, Camy-Peyret, C., Perrin, A., Goldman, A., Massie, S. T., Brown, L. R., and Toth, R. A.: The HITRAN molecular database: editions of 1991 and 1992, J. Quant. Spectrosc. Ra., 48, 469–507, 1992.

Rothman, L. S., Rinsland, C. P., Goldman, A., Massie, S. T., Edwards, D. P., Flaud, J.-M., Perrin, A., Camy-Peyret, C., Dana, V., Mandin, J.-Y., Schroeder, J., Mccann, A., Gamache, R. R., Wattson, R. B., Yoshino, K., Chance, K. V., Jucks, K. W., Brown, L. R., Nemtchinov, V., and Varanasi, P.: The HITRAN molecular spectroscopic database and HAWKS (HITRAN atmospheric workstation): 1996 edition, J. Quant. Spectrosc. Ra., 60, 665–710, 1998.

Rothman, L. S., Barbe, A., Benner, D. C., Brown, L. R., Camy-Peyret, C., Carleer, M. R., Chance, K., Clerbaux, C., Dana, V., Devi, V. M., Fayt, A., Flaud, J.-M., Gamache, R. R., Goldman, A., Jacquemart, D., Jucks, K. W., Lafferty, W. J., Mandin, J.-Y., Massie, S. T., Nemtchinov, V., Newnham, D. A., Perrin, A., Rinsland, C. P., Schroeder, J., Smith, K. M., Smith, M. A. H., Tang, K., Toth, R. A., Vander Auwera, J., Varanasi, P., and Yoshino, K.: The HITRAN molecular spectroscopic database: edition of 2000 including updates through 2001, J. Quant. Spectrosc. Ra., 82, 5–44, 2003.

Rothman, L. S., Jacquemart, D., Barbe, A., Chris Benner, D., Birk, M., Brown, L. R., Carleer, M. R., Chackerian Jr., C., Chance, K., Coudert, L. H., Dana, V., Devi, V. M., Flaud, J.-M., Gamache, R. R., Goldman, A., Hartmann, J.-M., Jucks, K. W., Maki, A. G.,

Mandin, J.-Y., Massie, S. T., Orphal, J., Perrin, A., Rinsland, C. P., Smith, M. A. H., Tennyson, J., Tolchenov, R. N., Toth, R. A., Vander Auwera, J., Varanasi, P., and Wagner, G.: The HITRAN 2004 molecular spectroscopic database, J. Quant. Spectrosc. Ra., 96, 139–204, 2005.

Ruhnke, R., Kouker, W., and Reddmann, T.: The influence of the OH+NO_2+M reaction on the NOy partitioning in the late arctic winter 1992/1993 as studied with KASIMA, J. Geophys. Res., 104, 3755–3772, 1999.

Sander, S. P., Friedl, R. R., Golden, D. M., Kurylo, M. J., Huie, R. E., Orkin, V. L., Moortgat, G. K., Ravishankara, A. R., Kolb, C. E., and Molina, M. J.: Chemical Kinetics and Photochemical Data for Use in Atmospheric Studies. Evaluation Number 14, JPL Publication 02-25, 2002.

Sander, R., Kerkweg, A., Jöckel, P., and Lelieveld, J.: Technical note: The new comprehensive atmospheric chemistry module MECCA, Atmos. Chem. Phys., 5, 445–450, doi:10.5194/acp-5-445-2005, 2005.

Sander, S. P., Friedl, R. R., Golden, D. M., Kurylo, M. J., Moortgat, G. K., Keller-Rudek, H., Wine, P. H., Ravishankara, A. R., Kolb, C. E., Molina, M. J., Finlayson-Pitts, B. J., Huie, R. E., Orkin, V. L.: Chemical Kinetics and Photochemical Data for Use in Atmospheric Studies. Evaluation Number 15, JPL Publication 06-2, Jet Propulsion Laboratory, Pasadena, USA, 2006.

Schneider, M., Blumenstock, T., Chipperfield, M. P., Hase, F., Kouker, W., Reddmann, T., Ruhnke, R., Cuevas, E., and Fischer, H.: Subtropical trace gas profiles determined by ground-based FTIR spectroscopy at Izaña (28° N, 16° W): Five-year record, error analysis, and comparison with 3-D CTMs, Atmos. Chem. Phys., 5, 153–167, doi:10.5194/acp-5-153-2005, 2005.

Schraner, M., Rozanov, E., Schnadt Poberaj, C., Kenzelmann, P., Fischer, A. M., Zubov, V., Luo, B. P., Hoyle, C. R., Egorova, T., Fueglistaler, S., Brönnimann, S., Schmutz, W., and Peter, T.: Technical Note: Chemistry-climate model SOCOL: version 2.0 with improved transport and chemistry/microphysics schemes, Atmos. Chem. Phys., 8, 5957–5974, doi:10.5194/acp-8-5957-2008, 2008.

Senten, C., De Mazière, M., Dils, B., Hermans, C., Kruglanski, M., Neefs, E., Scolas, F., Vandaele, A. C., Vanhaelewyn, G., Vigouroux, C., Carleer, M., Coheur, P. F., Fally, S., Barret, B., Baray, J. L., Delmas, R., Leveau, J., Metzger, J. M., Mahieu, E., Boone, C., Walker, K. A., Bernath, P. F., and Strong, K.: Technical Note: New ground-based FTIR measurements at Ile de La Réunion: observations, error analysis, and comparisons with independent data, Atmos. Chem. Phys., 8, 3483–3508, doi:10.5194/acp-8-3483-2008, 2008.

Sinnhuber, B.-M., Sheode, N., Sinnhuber, M., Chipperfield, M. P., and Feng, W.: The contribution of anthropogenic bromine emissions to past stratospheric ozone trends: a modelling study, Atmos. Chem. Phys., 9, 2863–2871, doi:10.5194/acp-9-2863-2009, 2009.

SPARC CCMVal: SPARC Report on the Evaluation of Chemistry-Climate Models, edited by: Eyring, V., Shepherd, T. G., Waugh, D. W., SPARC Report No. 5, WCRP-132, WMO/TD-No. 1526, http://www.atmosp.physics.utoronto.ca/SPARC, 2010.

Stiller, G. P., von Clarmann, T., Höpfner, M., Glatthor, N., Grabowski, U., Kellmann, S., Kleinert, A., Linden, A., Milz, M., Reddmann, T., Steck, T., Fischer, H., Funke, B., López-Puertas, M., and Engel, A.: Global distribution of mean age of stratospheric air from MIPAS SF6 measurements, Atmos. Chem. Phys., 8, 677–695, doi:10.5194/acp-8-677-2008, 2008.

Struthers, H., Bodeker, G. E., Smale, D., Rozanov, E., Schraner, M., and Peter, T.: Evaluating how photochemistry and transport determine stratospheric inorganic chlorine in coupled chemistry-climate models, Geophys. Res. Lett., 36, L04805, doi:10.1029/2008GL036403, 2009.

Sussmann, R. and Schäfer, K.: Infrared spectroscopy of tropospheric trace gases: combined analysis of horizontal and vertical column abundances, Appl. Optics, 36, 735–741, 1997.

Taylor, J. R., Wunch, D., Midwinter, C., Wiacek, A., Drummond, J. R., and Strong, K.: An extended intercomparison of simultaneous ground-based Fourier transform spectrometer measurements at the Toronto Atmospheric Observatory, J. Quant. Spectrosc. Ra., 109, 2244–2260, 2008.

Vigouroux, C., De Mazière, M., Demoulin, P., Servais, C., Hase, F., Blumenstock, T., Kramer, I., Schneider, M., Mellqvist, J., Strandberg, A., Velazco, V., Notholt, J., Sussmann, R., Stremme, W., Rockmann, A., Gardiner, T., Coleman, M., and Woods, P.: Evaluation of tropospheric and stratospheric ozone trends over Western Europe from ground-based FTIR network observations, Atmos. Chem. Phys., 8, 6865–6886, doi:10.5194/acp-8-6865-2008, 2008.

Wallace, L. and Livingston, W.: Spectroscopic observations of atmospheric trace gases over Kitt Peak, 3, Long-term trends of hydrogen chloride and hydrogen fluoride from 1978 to 1990, J. Geophys. Res., 96, 15513–15521, 1991.

Wallace, L., Livingston, W., and Hall, D. N. B.: A twenty-five year record of stratospheric hydrogen chloride, Geophys. Res. Lett., 24, 2363–2366, 1997.

Wallace, L., and Livingston, W. C.: Thirty-five year trend of hydrogen chloride amount above Kitt Peak, Arizona, Geophys. Res. Lett., 34, L16805, doi:10.1029/2007GL030123, 2007.

Washenfelder, R. A., Toon, G. C., Blavier, J.-F., Yang, Z., Allen, N. T., Wennberg, P. O., Vay, S. A., Matross, D. M., and Daube, B. C.: Carbon dioxide column abundances at the Wisconsin Tall Tower site, J. Geophys. Res.-Atmos., 111, D22305, doi:10.1029/2006JD007154, 2006.

Waugh, D. W., Strahan, S. E., and Newman, P. A.: Sensitivity of stratospheric inorganic chlorine to differences in transport, Atmos. Chem. Phys., 7, 4935–4941, doi:10.5194/acp-7-4935-2007, 2007.

Weatherhead, E. C., Reinsel, G. C., Tiao, G. C., Meng, X.-L., Choi, D., Cheang, W.-K., Keller, T., DeLuisi, J., Wuebbles, D. J., Kerr, J. B., Miller, A. J., Oltmans, S. J., and Frederick, J. E.: Factors affecting the detection of trends: Statistical considerations and applications to environmental data, J. Geophys. Res., 103, 17149–17161, 1998.

Wiacek, A., Taylor, J. R., Strong, K., Saari, R., Kerzenmacher, T. E., Jones, N., and Griffith, D. W. T.: Ground-based solar absorption FTIR spectroscopy: a novel optical design instrument at a new NDSC complementary station, characterization of retrievals and first results, J. Atmos. Ocean. Technol., 24, 432–448, 2007.

WMO (World Meteorological Organization): Scientific Assessment of Ozone Depletion: 2002, Global ozone research and monitoring project, Report No. 47, Geneva, Switzerland, 2003.

WMO (World Meteorological Organization): Scientific Assessment of Ozone Depletion: 2006, Global Ozone Research and Monitoring Project, Report No. 50, Geneva, Switzerland, 2007.

WMO (World Meteorological Organization): Scientific Assessment of Ozone Depletion: 2010, Global Ozone Research and Monitoring Project, Report No. 52, Geneva, Switzerland, 2011.

Wunch, D., Taylor, J. R., Fu, D., Bernath, P., Drummond, J. R., Midwinter, C., Strong, K., and Walker, K. A.: Simultaneous ground-based observations of O_3, HCl, N_2O, and CH_4 over Toronto, Canada by three Fourier transform spectrometers with different resolutions, Atmos. Chem. Phys., 7, 1275–1292, doi:10.5194/acp-7-1275-2007, 2007.

Zander, R., Roland, G., Delbouille, L., Saval, A., Farmer, C. B., and Norton, R. H.: Column abundance and the long-term trend of hydrogen chloride (HCl) above the Jungfraujoch station, J. Atmos. Chem., 5, 395–404, 1987.

Zander, R., Mahieu, E., Demoulin, P., Duchatelet, P., Roland, G., Servais, C., De Mazière, M., Reimann, S., and Rinsland, C. P.: Our changing atmosphere: Evidence based on long-term infrared solar observations at the Jungfraujoch since 1950, Sci. Total Environ., 391, 184–195, 2008.

Supplement to:

Observed and simulated time evolution of HCl, $ClONO_2$, and HF total column abundances

Atmos. Chem. Phys., 2012

by R. Kohlhepp et al.

15 March 2012

Table 1: Overview of the measurement specifications for HCl.

Measurement site	Spectral resolution [cm^{-1}]	Spectral microwindows [cm^{-1}]	Retrieved interfering species	Source of p/T profiles	Retrieval code	Spectroscopic database	Reference
Eureka DA8 (1997-2006)	0.004	2925.70-2926.10	NO_2	radiosondes, NCEP, US Sub-Arctic Winter Model	SFIT1.09e	HITRAN 1992 plus updates	Fast et al. (2011)
Eureka 125HR (2006-2009)	0.0035	2775.72-2775.80 2821.40-2821.62 2925.75-2926.05	O_3, CH_4, N_2O; HDO, N_2O; CH_4, NO_2, OCS, O_3	radiosondes, NCEP, US St. Atm.	SFIT2 v3.92C	HITRAN 2004 plus updates	Batchelor et al. (2009)
Ny Ålesund	0.005	2925.65-2926.25	CH_4	NCEP	GFIT	updated ATMOS linelist from GFIT package, v2.6.4	Notholt et al. (1995b)
Thule	0.0035	2727.60-2727.95 2775.60-2775.95 2925.70-2926.10	O_3, CH_4, HDO	NCEP	SFIT2 v3.93	HITRAN 2004 plus updates to 2007	Hannigan et al. (2009)
Kiruna	0.005	2727.73-2727.82 2775.73-2775.79 2819.52-2819.61 2821.52-2821.62 2843.60-2843.65 2904.09-2904.14 2923.65-2923.78 2925.80-2926.00 2942.70-2942.75 2961.04-2961.09 2963.25-2963.32 2995.76-2995.79	H_2O, O_3, CH_4	NCEP	PROFFIT	HITRAN 2004	Blumenstock et al. (2006)
Poker Flat	0.0035	2925.80-2926.00	H_2O, CH_4, NO_2, O_3	radiosondes, UKMO, CIRA86	SFIT2 v3.7	HITRAN 2004	Kagawa et al. (2007)
Harestua		2925.60-2926.20 2925.75-2926.00	H_2O, CH_4, NO_2, HCl, O_3	NCEP	SFIT2 v3.81	HITRAN 2004	
Zugspitze	0.005	2925.74-2926.06	CH_4	Munich radiosonde	SFIT1.09e	HITRAN 1996	Sussmann and Schäfer (1997)
Jungfraujoch	0.003	2925.74-2926.06	CH_4, NO_2	NCEP	SFIT1.09c	HITRAN 1992	Rinsland et al. (2003)
Toronto	0.004	2925.80-2926.00	CH_4, NO_2, O_3	NCEP, US St. Atm.	SFIT2 v3.82B3	HITRAN 2004	Wiacek et al. (2007)
Tsukuba	0.0035	2925.69-2926.21	CH_4, H_2O	radiosondes at Tateno	SFIT1.09e	HITRAN 1996	Murata et al. (2005)
Izaña	0.0036	same as Kiruna	H_2O, O_3, CH_4	local radiosondes	PROFFIT	HITRAN 2004	Schneider et al. (2005)
Mauna Loa	0.0035	2925.69-2926.50	CH_4	radiosondes at Hilo	SFIT1	HITRAN 2000	Hannigan et al. (2009)
La Réunion	0.00513 and 0.00893	2925.70-2926.10	CH_4	NCEP	SFIT2 v3.9	HITRAN 2004 plus updates for H_2O, N_2O, HNO_3, C_2H_6	Senten et al. (2008)
Wollongong	0.0035	2925.80-2926.00	CH_4	NCEP	GFIT	HITRAN 2004	Rinsland et al. (2003)
Lauder	0.0035	2925.75-2926.05	CH_4, NO_2, H_2O, O_3	NCEP/ NCAR	SFIT2 v3.82B3	HITRAN 2000	Rinsland et al. (2003)
Arrival Heights	0.0035	2925.75-2926.05	CH_4, NO_2, H_2O, O_3	NCEP/ NCAR	SFIT2 v3.82B3	HITRAN 2000	Mahieu et al. (2008)

Table 2: Overview of the measurement specifications for $ClONO_2$.

Measurement site	Spectral resolution [cm^{-1}]	Spectral microwindows [cm^{-1}]	Retrieved interfering species	Source of p/T profiles	Retrieval code	Spectroscopic database	Reference
Eureka DA8 (1997-2006)	0.004	779.550-781.100	O_3, H_2O, CO_2, C_2H_2	radiosondes, NCEP, US Sub-Arctic Winter Model	SFIT1.09e	HITRAN 1992 plus updates	Fast et al. (2011)
Eureka 125HR (2006-2009)	0.0035	779.850-780.450 782.550-782.870 938.300-939.300	CO_2, O_3, HNO_3; O_3, CO_2, H_2O, HNO_3; CO_2	radiosondes, NCEP, US St. Atm.	SFIT2 v3.92C	HITRAN 2004 plus updates	Batchelor et al. (2009)
Ny Ålesund	0.005	778.640-782.800	O_3, CO_2, H_2O, C_2H_2	NCEP	GFIT	updated ATMOS-linelist from GFIT package, v2.6.4	Notholt et al. (1995b)
Thule	0.01	780.120-780.320 780.700-781.250	O_3, CO_2	NCEP	SFIT2 v3.93	HITRAN 2004 plus updates to 2007	Hannigan et al. (2009)
Kiruna	0.005	779.000-779.800 780.000-780.300 780.300-781.300	H_2O, CO_2, O_3, HNO_3, C_2H_2	NCEP	PROFFIT	HITRAN 2004	Blumenstock et al. (2006)
Harestua		779.500-780.700 779.905-780.340	CO_2, H_2O, O_3, $ClONO_2$, HNO_3	NCEP	SFIT2 v3.81	HITRAN 2004	
Zugspitze	0.0036	779.300-780.600 780.050-780.355	H_2O, O_3, CO_2	Munich radiosonde	SFIT2 v3.8	HITRAN 1996 with Birk parameters for $ClONO_2$	Sussmann and Schäfer (1997)
Jungfraujoch	0.005	779.300-780.600 780.050-780.355	Wide: H_2O, O_3, CO_2; Narrow: O_3, HNO_3, COF_2	NCEP	SFIT2 v3.81	HITRAN 1996 including Birk and Wagner line parameters	Rinsland et al. (2003)
Izaña	0.0036	779.000-779.800 780.000-780.300 780.300-781.300	H_2O, CO_2, O_3, HNO_3, C_2H_2	local radiosondes	PROFFIT	HITRAN 2004	Schneider et al. (2005)
Wollongong	0.0035	779.300-780.600 780.050-780.355	Wide: O_3, H_2O, CO_2, C_2H_2; Narrow: none	NCEP	SFIT2 v3.92	HITRAN 2004	Rinsland et al. (2003)
Lauder	0.0035	779.300-780.600 780.050-780.355	Wide: O_3, H_2O, CO_2, C_2H_2; Narrow: none	NCEP/ NCAR	SFIT2 v3.82B3	HITRAN 2000	Rinsland et al. (2003)
Arrival Heights	0.0035	779.300-780.600 780.050-780.355	Wide: O_3, H_2O, CO_2, C_2H_2; Narrow: none	NCEP/ NCAR	SFIT2 v3.82B3	HITRAN 2000	Rinsland et al. (2003)

Table 3: Overview of the measurement specifications for HF.

Measurement site	Spectral resolution [cm^{-1}]	Spectral microwindows [cm^{-1}]	Retrieved interfering species	Source of p/T profiles	Retrieval code	Spectroscopic database	Reference
Eureka DA8 (1997-2006)	0.004	4038.780-4039.100	H_2O	radiosondes, NCEP, US Sub-Arctic Winter Model	SFIT1.09e	HITRAN 1992 plus updates	Fast et al. (2011)
Eureka 125HR (2006-2009)	0.0035	4038.780-4039.100	H_2O, HDO, CH_4	radiosondes, NCEP, US St. Atm.	SFIT2 v3.92C	HITRAN 2004 plus updates	Batchelor et al. (2009)
Ny Ålesund	0.005	4038.600-4039.240	H_2O	NCEP	GFIT	updated ATMOS-linelist from GFIT package, v2.6.4	Notholt et al. (1995a)
Thule	0.0035	4000.800-4001.200 4038.750-4039.200	H_2O, CH_4, HDO	NCEP	SFIT2 v3.93	HITRAN 2004 plus updates to 2007	Hannigan et al. (2009)
Kiruna	0.0075	4000.900-4001.050 4038.850-4039.080	H_2O	NCEP	PROFFIT	HITRAN 2004	Blumenstock et al. (2006)
Poker Flat	0.0035	4038.804-4039.148	H_2O	radiosondes, UKMO, CIRA86	SFIT2 v3.7	HITRAN 2004	Kagawa et al. (2007)
Harestua		4038.100-4039.500 4038.860-4039.050	H_2O, HDO, CH_4, HF	NCEP	SFIT2 v3.81	HITRAN 2004	
Zugspitze	0.0078	4038.800-4039.100	H_2O column	Munich Radiosonde	SFIT1.09e	HITRAN 1996	Sussmann and Schäfer (1997)
Jungfraujoch	0.004	4038.800-4039.105	CH_4, NO_2	NCEP	SFIT1.09c	HITRAN 1992	Zander et al. (2008)
Toronto	0.004	4038.770-4039.130	H_2O, HDO, CH_4	NCEP, US St. Atm.	SFIT2 v3.82B3	HITRAN 2004	Wiacek et al. (2007)
Tsukuba	0.0035	4038.800-4039.100	H_2O, HDO, CH_4	radiosonde	SFIT1.09e	HITRAN 1996	Murata et al. (2005)
Izaña	0.0036	4000.900-4001.050 4038.850-4039.080	H_2O	local radiosondes	PROFFIT	HITRAN 2004	Schneider et al. (2005)
Mauna Loa	0.0035	4038.850-4039.050	H_2O	radiosondes at Hilo	SFIT1	HITRAN 2000	Hannigan et al. (2009)
La Réunion	0.0072	4038.700-4039.050	H_2O	NCEP	SFIT2 v3.9	HITRAN 2004 updates for H_2O, N_2O, HNO_3, C_2H_6	Senten et al. (2008)
Wollongong	0.0035	4038.810-4039.090	H_2O	NCEP	GFIT	HITRAN 2004	Mahieu et al. (2008)
Lauder	0.0035	4038.780-4039.0995	H_2O, HDO, CH_4	NCEP/ NCAR	SFIT2 v3.82B3	HITRAN 2000	Reisinger et al. (1994)
Arrival Heights	0.0035	4038.780-4039.100	H_2O, HDO, CH_4	NCEP/ NCAR	SFIT2 v3.82B3	HITRAN 2000	Reisinger et al. (1994)